JOINT TRANSPORTATION
RESEARCH PROGRAM
INDIANA DEPARTMENT OF TRANSPORTATION
AND PURDUE UNIVERSITY

Resilient Modulus Improvements to Bases and Subgrades From Geosynthetic Reinforcement

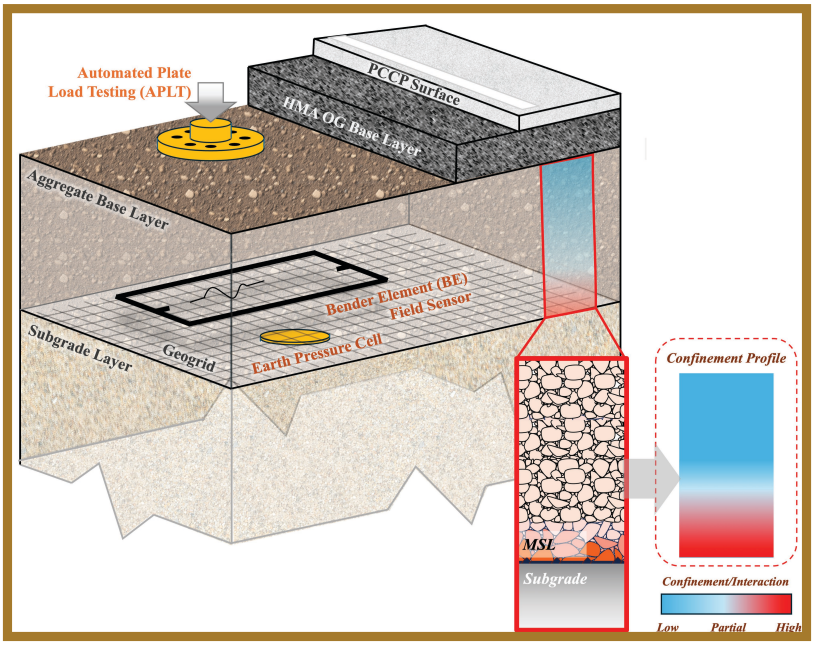

Syed Faizan Husain, Issam I. A. Qamhia, Erol Tutumluer, and Peter J. Becker

SPR-4723 • Report Number: FHWA/IN/JTRP-2025/37 • DOI: 10.5703/1288284318600

RECOMMENDED CITATION

Husain, S. F., Qamhia, I. I. A., Tutumluer, E., & Becker, P. J. (2025). *Resilient modulus improvements to bases and subgrades from geosynthetic reinforcement* (Joint Transportation Research Program Publication No. FHWA/IN/JTRP-2025/37). West Lafayette, IN: Purdue University. https://doi.org/10.5703/1288284318600

AUTHORS

Syed Faizan Husain, PhD
University of Illinois Urbana-Champaign

Issam I.A. Qamhia, PhD
University of Illinois Urbana-Champaign

Erol Tutumluer, PhD
University of Illinois Urbana-Champaign
tutumlue@illinois.edu
Corresponding Author

Peter J. Becker, PhD, PE
Indiana Department of Transportation

JOINT TRANSPORTATION RESEARCH PROGRAM

The Joint Transportation Research Program serves as a vehicle for INDOT collaboration with higher education institutions and industry in Indiana to facilitate innovation that results in continuous improvement in the planning, design, construction, operation, management and economic efficiency of the Indiana transportation infrastructure. Learn more at engineering.purdue.edu/JTRP.

Published reports of the Joint Transportation Research Program are available at docs.lib.purdue.edu/jtrp/.

NOTICE

TECHNICAL REPORT DOCUMENTATION PAGE

1. Report No.	2. Government Accession No.	3. Recipient's Catalog No.
FHWA/IN/JTRP-2025/37		

4. Title and Subtitle	5. Report Date
Resilient modulus improvements to bases and subgrades from geosynthetic reinforcement	December 9, 2025
	6. Performing Organization Code

7. Author(s)	8. Performing Organization Report No.
Syed Faizan Husain, PhD (https://orcid.org/0000-0003-1015-5885) Issam I. A. Qamhia, PhD (https://orcid.org/0000-0002-2020-8437) Erol Tutumluer, PhD (https://orcid.org/0000-0003-3945-167X) Peter J. Becker, PhD, PE (https://orcid.org/0000-0003-0283-8248)	FHWA/IN/JTRP-2025/37

9. Performing Organization Name and Address	10. Work Unit No.
Joint Transportation Research Program Hall for Discovery and Learning Research (DLR), Suite 204 207 S. Martin Jischke Drive West Lafayette, IN 47907	**11. Contract or Grant No.** SPR-4723

12. Sponsoring Agency Name and Address	13. Type of Report and Period Covered
Indiana Department of Transportation (SPR) State Office Building 100 North Senate Avenue Indianapolis, IN 46204	Final Report
	14. Sponsoring Agency Code

15. Supplementary Notes

Conducted in cooperation with the U.S. Department of Transportation, Federal Highway Administration.

16. Abstract

This study investigated the benefits of geogrid stabilization in unbound granular layers and developed a framework to incorporate those benefits into mechanistic–empirical (ME) pavement design. The purpose was to address limitations in current design practices that treat geosynthetic stabilized and non-stabilized layer equivalently, despite evidence of enhanced stiffness and improved stress distribution from a geogrid inclusion. Field testing was conducted along US 20 in Indiana using Automated Plate Load Testing (APLT) device during the construction of three full-scale pavement test sections: control (CS), geogrid installed at the unbound granular layer-subgrade interface (GG1), and geogrid installed at mid-depth (GG2) of unbound granular layer. Pavement instrumentation included Bender Element (BE) shear wave transducer field sensors, earth pressure cells and moisture and temperature sensors. APLT-derived modulus and BE sensor shear wave velocity measurements confirmed increased stiffness in geogrid-stabilized sections, with up to 23% higher local stiffness observed due to pulsed stresses. Further, long-term monitoring of BE sensor data under traffic loading through seasonal changes confirmed geogrid's effectiveness in reducing base layer modulus reduction. A sublayer-based finite element (FE) modeling approach was developed to translate these findings as inputs into the ME pavement design framework. In accordance, the 12-in. thick base courses were discretized into six 2-in. sublayers and characterized using nonlinear, stress-dependent resilient modulus model parameters (k_1, k_2, k_3) calibrated using field data and applied through depth-specific scalar multipliers to represent the mechanically stabilized layer (MSL). The FE analysis results closely matched measured deflections, strains, and stresses, confirming the reliability of the calibrated approach. A parametric study across typical INDOT pavement sections showed that mid-depth geogrid placement (GG2) provided the greatest reduction in subgrade deviator strain and stress. These findings indicate that geogrid stabilization can be effectively represented within the ME pavement design framework using localized modulus enhancements associated with the MSL concept. Agencies can use the current research approach and the ME design framework to inform design decisions to quantify benefits and develop specification guidelines for geogrid-stabilized aggregate bases.

17. Key Words	18. Distribution Statement
geogrid stabilization, mechanistic-empirical pavement design, aggregate material, stress-dependent stiffness, pavement design, input calibration	No restrictions. This document is available through the National Technical Information Service, Springfield, VA 22161.

19. Security Classif. (of this report)	20. Security Classif. (of this page)	21. No. of Pages	22. Price
Unclassified	Unclassified	44, including appendices	

EXECUTIVE SUMMARY

Introduction

Response and performance evaluations and related design benefits of geogrid stabilization in unbound aggregate layers have been studied for Indiana paved roads as part of the Indiana Department of Transportation (INDOT) SPR-4723 research project. The current AASHTOWare Pavement Mechanistic–Empirical Design (PMED), as implemented in the state of Indiana, rely on overly conservative assumptions while designing geosynthetic-stabilized pavement layers. As a result, stabilization effects are neglected, and the unbound granular layers (referred to as "aggregate base" throughout the report) is often modeled as a nonstabilized aggregate without appropriate consideration for the benefits of a mechanically stabilized layer (MSL) commonly associated with a geogrid inclusion. These limitations have been addressed through a rigorous in-situ testing and evaluation research effort in a road reconstruction project on U.S. Route 20 (US 20) in Elkhart County, Indiana, for quantifying stiffness improvements and stress distribution behavior in geogrid-stabilized pavement base courses. A data informed modeling framework is also developed to integrate these benefits into the mechanistic–empirical (ME) pavement design methodology.

The primary objective of this research was to quantify the performance advantages offered by geogrid stabilization under field conditions that reflect actual traffic loading and seasonal environmental changes. Through extensive field testing and use of embedded sensor data, the study sought to establish the MSL role of a biaxial geogrid, when placed in mid-depth and at bottom of base, for improving repeated load response, preserving base stiffness over time, and mitigating overstressing the subgrade. A secondary objective was to translate these observations into resilient modulus (M_R) inputs for the base course through a sublayering method applicable to the ME design framework.

Findings

Field testing revealed a measurable benefit attributable to geogrid stabilization that was associated with improved repeated load response behavior and localized stiffness gains in the aggregate bases. Measurements from Bender Element (BE) shear wave transducer field sensors indicated up to 30% increase in layer modulus in geogrid-stabilized sections compared to the nonstabilized control section. These improvements were particularly pronounced in near geogrid zone-of-influence. Automated Plate Load Testing (APLT) was performed, and earth pressure cell data was collected during repeated load applications further demonstrating that geogrid inclusion consistently reduced the magnitude of vertical stress transmitted on subgrade.

Over the course of one year of monitoring and as measured with BE field sensors, geogrid-stabilized layers maintained or improved their stiffness, while the control section exhibited progressive stiffness degradation. Furthermore, during spring thaw conditions under which pavement foundation performance is typically most vulnerable, stress transmission on subgrade was minimized consistently in sections with geogrid stabilization at mid-depth of the aggregate layer. These findings confirm and quantify benefits of MSL and its retention of pavement foundation performance attributes under the effect of traffic and environmental loadings.

Implementation

To implement these quantifiable response and performance benefits into pavement design practice, a finite element (FE) modeling-based framework was developed by incorporating the in-situ testing and sensor data into the U.S. Army Corps of Engineers's Flexible Pavement Analysis (C-FLEX) solution engine. The C-FLEX FE analysis modeled the full-scale pavement test section geometry and layer material characterizations by properly incorporating nonlinear, stress-dependent resilient modulus behavior in the base courses studied. To represent the MSL in the geogrid-stabilized sections, the aggregate base layer was discretized into sublayers, and each sublayer was assigned the Mechanistic–Empirical Pavement Design Guide (MEPDG) resilient modulus model parameters calibrated to predict the measured pavement responses under APLT. These MEPDG model parameters could accurately predict the load response behavior of the aggregate bases including stiffness characteristics and stress sensitivities. The MEPDG M_R model parameters were first derived for the control section from the APLT data of the unbound aggregate layer. Then, geogrid influence zones were taken into consideration and modelled by adjusting the unbound aggregate M_R model parameters using scalar multipliers to simulate varying degrees of localized stiffness increases associated with the geogrid-aggregate interlock controlling the MSL. Finally, the FE analysis results were validated by matching them against the field-measured deflections and shear wave velocity data.

The integration of field instrumentation with the sublayering approach offers a path forward for incorporating the benefits of geogrid stabilization into routine design practice. While current Pavement Mechanistic–Empirical Design (PMED) limits the number of layers that can be modeled, future iterations are recommended to incorporate multilayer modeling. The MSL concept can also be accounted for in the analysis for ME design by assigning enhanced MEPDG M_R model parameters to the base layer in a similar manner reported for sublayers in the study, although the gradual increase/decrease towards/away from the geogrid location would not be properly modeled then. The findings from C-FLEX FE analyses, referred to herein as the parametric study on typical INDOT pavement systems, indicated geogrid placement at either the mid-depth of the base or the base–subgrade interface can reduce critical pavement response, resulting in quantifiable modulus enhancement ratios. These ratios reflect not only immediate performance gains but also the potential for extended service life and improved pavement durability when paired with stiffness retention observations made with BE field sensors from the experimental sections on US 20 over the monitoring period.

Overall, the study provides a comprehensive data-informed methodology for quantifying, modeling, and implementing geogrid benefits in pavement foundations. The findings support the incorporation of geogrid effects into INDOT's ME design framework and offer guidance for future research and implementation.

CONTENTS

LIST OF TABLES

LIST OF FIGURES

1. INTRODUCTION

1.1 Background and Problem Statement

Aggregate base layers are a critical component of pavement systems, providing structural support, load distribution, and drainage for overlying asphalt and concrete surfaces. The long-term performance of these layers under repeated traffic loading and environmental stressors depends on their ability to retain stiffness and resist deformation. In unbound aggregate materials, stiffness is not constant but varies with traffic-induced stress levels, confinement conditions, and moisture content. These factors create challenges for pavement engineers seeking to accurately characterize layer behavior in support of mechanistic–empirical (ME) design procedures. To improve the performance and service life of aggregate base layers, geosynthetic stabilization, particularly with geogrids, has gained widespread interest. Geogrids are engineered materials with an open aperture structure that enable enhanced mechanical interlock within aggregate base layers. When placed strategically within the base course, geogrids can restrain lateral aggregate movement, reduce deformation, and enhance load distribution. While these benefits have been demonstrated in laboratory testing and accelerated pavement test tracks (Al-Qadi et al., 2006; Byun & Tutumluer, 2017; Giroud, 2009; Kwon et al., 2009), there remains considerable uncertainty about how to quantify pavement response and performance effects in full-scale field evaluations and associated with proper mechanical stabilization mechanisms, especially in a way that is compatible with current pavement design practices used by the Indiana Department of Transportation (INDOT).

Current INDOT pavement analysis and design consideration for unbound aggregate base layers rely on inputting a fixed resilient modulus (M_R) of 15 ksi, selected conservatively without accounting for layer mechanical stabilization benefits, in AASHTOWare Pavement ME Design software. Use of the same modulus value for both the geogrid-stabilized and nonstabilized unbound aggregate layers results in an underutilization of the improved structural layer characteristics by a geogrid inclusion. The lack of mechanistic guidance on how to adjust M_R values based on geogrid placement depth, or field conditions remains a key barrier to the wider adoption of geogrid stabilization in INDOT pavement systems.

Part of the impediment to wider optimal design practices lies in the limitations of existing field evaluation tools. Traditional surface deflection measurements, such as those obtained using a Falling Weight Deflectometer (FWD), provide an overview of pavement response but lack the depth profile spatial resolution and sensitivity required to isolate the effects of geogrid stabilization within the base layer. Moreover, these tests typically rely on unrealistic assumptions during estimation of layer moduli values instead of a direct measurement. Therefore, embedded sensing technologies that can directly measure changes in local stiffness and stress distribution within the aggregate base, particularly near the geogrid layer, are gaining interest among the pavement research and professional communities. This research project implements an in-situ testing and sensor data informed approach at a full-scale in-service road section constructed as part of the U.S. Route 20 (US 20) reconstruction project in Elkhart County, Indiana. The study integrates repeated loading tests using an Automated Plate Load Testing (APLT) device with embedded Bender Element (BE) field sensors and subgrade pressure cells toward capturing local stiffness characteristics and critical pavement responses under varying load and environmental conditions.

Through the field evaluation paired with calibrated finite element method analyses scheme, the project sought to quantify the benefits of geogrid mechanical stabilization and to develop a framework for incorporating these findings into INDOT's pavement design procedures. By translating observed improvements in aggregate subgrade (referred to as "aggregate base" or "base" throughout the rest of the report) layer stiffness or modulus behavior, and reduction of subgrade vertical stress into actionable design inputs, this work aims to support more accurate pavement designs that recognize the value of geosynthetic stabilization. The findings are intended to reduce uncertainty in current practice, improve the representation of base layer performance in ME design, and provide INDOT with a roadmap for implementing geogrid technologies in a systematic and evidence-based manner.

1.2 Objectives and Scope

The overarching objective of this research project was to quantify the resilient modulus improvement in pavement base layers due to geogrid stabilization under in-service traffic loading and environmental conditions. The study focused on evaluating local and composite stiffness characteristics of unbound aggregate base layers constructed with and without geogrid stabilization, with the goal of enhancing the mechanistic analysis tools and a better understanding of stiffness evolution and load distribution behavior in such systems.

To achieve this, a full-scale experimental site was constructed along a reconstructed segment of US 20 in Elkhart County, Indiana. The site included three test sections: a control section with no geogrid and two geogrid-stabilized sections where geogrids were placed either at the base–subgrade interface or at mid-depth within the aggregate base layer. These sections were instrumented with embedded BE field sensors and earth pressure cells to measure changes in stiffness and subgrade vertical stress over time and relate the measurements to seasonal and environmental changes through moisture and temperature sensor data also collected from the field experiments. The specific objectives of the study were to:

1. Establish baseline stiffness properties of geogrid-stabilized and nonstabilized base layers immediately after construction using BE sensors and APLT-derived composite moduli.
2. Characterize resilient modulus behavior of base layers through paired instrumentation and surface deflection measurements under varying stress states.
3. Assess stress-dependent layer stiffness trends to determine the influence of geogrid inclusion on modulus enhancement across a range of loading conditions.

4. Monitor seasonal/environmental conditions and traffic-induced changes in pavement foundation response through long-term pressure cell and BE sensor data collection.
5. Develop design recommendations for incorporating geogrid stabilization effects into INDOT ME design practices, including the proposed resilient modulus enhancement ratios for different geogrid configurations.

1.3 Organization of the Report

This report is organized into six chapters, each addressing a critical component of the research and its relevance to pavement design practices in Indiana. The structure reflects the logical flow of the project from its motivation and technical foundation through implementation-focused conclusions.

- *Chapter 1–Introduction:* Outlines the motivation for the study, defines the project objectives, and presents the scope of work. It also introduces the organizational structure of the report.
- *Chapter 2–Literature Review:* Summarizes existing research and technical knowledge relevant to geogrid stabilization, stiffness characterization methods for unbound materials, and the application of specialized instrumentation such as BE sensors and APLT device. The chapter identifies critical gaps in current standards and practice that this study seeks to address.
- *Chapter 3–Construction of Pavement Test Sections:* Details the development of full-scale test sections constructed along US 20 in Elkhart County. The chapter describes the pavement structure, geogrid placement configurations, instrumentation layout, and data acquisition procedures used to monitor early-age and long-term pavement foundation response.
- *Chapter 4–Research Findings:* Presents the results of preliminary and long-term performance evaluations, including dynamic cone penetrometer (DCP) and light weight deflectometer (LWD)-based site characterization, analysis of repeated load APLT and earth pressure cell data, and interpretation of stiffness trends captured through BE sensors. This chapter highlights stress dependent modulus behavior and evaluates changes in response under seasonal and traffic-induced loading.
- *Chapter 5–Implementation of Research Results:* Translates the findings into practical guidance for INDOT implementation. It proposes enhancement ratios for resilient modulus input in geogrid-stabilized base layers, introduces a mechanistic framework for representing mechanically stabilized layers, and discusses implications for typical INDOT pavement configurations.
- *Chapter 6–Conclusions and Recommendations:* Summarizes the study's major findings and their relevance to improving pavement design accuracy and material selection strategies. Recommendations for INDOT practice and future research directions are provided to support the ongoing integration of geogrid stabilization into agency specifications and modeling platforms.

2. LITERATURE REVIEW

A comprehensive understanding of the mechanical behavior of pavement foundation layers is essential for the development of effective design practices, particularly when incorporating innovative stabilization techniques such as geogrid stabilization. Over the past two decades, the transportation geotechnics community has produced a substantial body of research exploring the performance, benefits, and limitations of geogrid-stabilized unbound aggregate layers. This chapter synthesizes relevant literature to provide a technical foundation for the present study and to frame its contribution within the broader context of ME pavement design.

2.1 Mechanisms of Geogrid Stabilization in Pavement Bases

Geogrid stabilization of unbound aggregate base layers is increasingly recognized as a viable means of improving pavement foundation performance. The underlying mechanisms by which geogrids enhance structural response are rooted in their ability to interact mechanically with surrounding aggregate particles, resulting in improved load distribution, increased confinement, and localized stiffness enhancement. These improvements are particularly relevant under traffic-induced loading, where repeated shear stresses tend to induce permanent deformation in untreated granular layers (Tutumluer, 2008).

When placed within or at the interface of an aggregate base layer, geogrids function as in-plane stabilization elements that resist lateral movement of aggregate particles. This restriction of lateral displacement, often described as a "confinement effect," increases the aggregate layer's load-carrying capacity by promoting a denser, more interlocked structure (Qamhia & Tutumluer, 2021; Zornberg, 2012). The geogrid's aperture geometry and tensile stiffness contribute to the development of passive resistance against particle movement, thereby reducing the potential for shear-induced deformation. This behavior has been well documented in laboratory and full-scale studies, which consistently report reductions in vertical and lateral strains in geogrid-stabilized sections compared to unstabilized controls (Byun et al., 2023; Kwon et al., 2009; Leonardi et al., 2020).

Another critical mechanism involves the formation of a mechanically stabilized layer (MSL), characterized by a zone of increased stiffness and reduced stress sensitivity surrounding the geogrid inclusion. The development of the MSL is influenced by geogrid placement depth, aggregate gradation, compaction quality, and the stiffness of underlying subgrade materials (H. Lee, 2017; Qamhia & Tutumluer, 2021). The enhanced performance attributed to the MSL is not merely a result of increased modulus but also a function of improved aggregate structure, reduced particle reorientation under load, and better preservation of layer integrity over time (Zornberg, 2012).

Numerical and analytical studies further support these findings by demonstrating that geogrid-stabilized bases exhibit modified stress paths and attenuate load transmission to the subgrade (Kwon & Tutumluer, 2009). These modifications can reduce critical pavement responses, such as vertical subgrade strain or stress, which is directly linked to rutting as a long-term pavement performance indicator. However, despite these benefits, geogrid-stabilized systems remain underutilized in mechanistic–empirical design frameworks due to limited guidance on quantifying their effects in terms of resilient modulus or other standard inputs (Giroud, 2009).

2.2 Interlocking and Confinement Effects

Interlocking and confinement are two fundamental mechanisms through which geogrid stabilization improves the mechanical behavior of unbound aggregate base layers. These mechanisms operate simultaneously to enhance aggregate particle interaction and restrict deformation under traffic-induced stresses. Their contribution to improved pavement performance has been substantiated through experimental studies, mechanistic modeling, and field observations (Al-Qadi et al., 2012; Byun & Tutumluer, 2017; Husain et al., 2024; Leonardi et al., 2020; Suku et al., 2017).

Interlocking refers to the mechanical engagement that occurs when angular aggregate particles strikethrough and bear against the apertures of a geogrid. This interaction transfers load from the aggregate to the geogrid, enabling tensile forces to develop within the geosynthetic. The extent of interlocking is influenced by the relative size and shape of the aggregate particles, the aperture geometry of the geogrid, and the method of installation. For instance, open-aperture geogrids with a high rib stiffness and appropriate junction integrity provide better mechanical interlock than flexible, fine-mesh materials. When properly embedded, the geogrid promotes a stable aggregate skeleton by inhibiting particle rotation and translation, which in turn reduces strain accumulation under repeated loading (Husain et al., 2024; H. Lee, 2017; Liu et al., 2016).

Confinement, on the other hand, results from the lateral restraint imposed by the geogrid on the surrounding aggregate. As vertical loading is applied on the pavement surface, aggregate particles tend to move outward and downward. A geogrid placed within or at the bottom of the base layer disrupts this movement by providing lateral stiffness, thereby generating a confinement that reduces deformation of the aggregate mass. This lateral confinement increases the shear strength of the base layer and delays the onset of plastic deformation. Furthermore, the confinement effect contributes to a stiffer, more stable base layer that is better able to resist rutting and distribute loads over a broader area of the subgrade (Husain et al., 2025; Kwon et al., 2009; Wayne et al., 2011).

These mechanisms are not isolated in practice. Rather, they operate synergistically to develop what is often referred to as an MSL. The MSL exhibits distinct material behavior characterized by enhanced stiffness, reduced stress sensitivity, and a higher resistance to permanent deformation. Laboratory cyclic triaxial and full-scale pavement tests have both demonstrated that geogrid-stabilized sections show marked reductions in permanent strain accumulation and improved resilient response compared to unstabilized controls (H. Lee, 2017; Nazzal, 2007).

It is important to note that the efficacy of interlocking and confinement is dependent on proper construction practices, including appropriate placement depth, adequate compaction, and control of particle size distribution (Wang et al., 2023). Misplacement or poor aggregate-geogrid contact can significantly reduce the magnitude of stabilization benefits. Therefore, a robust understanding of these mechanisms is essential for translating laboratory-scale insights into effective field applications and for informing ME design strategies that aim to incorporate geosynthetic stabilization effects.

2.3 Characterization of Pavement Foundation Stiffness

Accurate characterization of the stiffness of pavement foundation layers is essential for ME pavement design. Foundation stiffness influences stress distribution, deflection behavior, and long-term pavement performance under repeated traffic and environmental loading. In particular, the M_R has emerged as the main input property that represents the elastic response of unbound aggregate bases and subgrade soils under repeated loading conditions (Seyhan & Tutumluer, 2002; Tutumluer & Seyhan, 1999). Defined as the ratio of recoverable stress to recoverable strain, the resilient modulus captures the nonlinear, stress-dependent behavior of geomaterials, allowing for more accurate modeling of layered pavement systems.

Traditional methods for stiffness characterization often rely on laboratory repeated load triaxial (RLT) testing, conducted in accordance with AASHTO T 307 or similar standards. While such tests provide valuable insight into the stress-strain response of unbound materials under controlled conditions, they do not always capture the complex in-situ conditions encountered in the field, including construction variability, boundary confinement, and moisture fluctuations (Hicks & Monismith, 1971; Seed et al., 1967; Seyhan & Tutumluer, 2002; Tutumluer & Seyhan, 1999). Furthermore, laboratory-prepared specimens may not accurately replicate the aggregate structure or particle interlock achieved during field compaction, especially in stabilized layers.

To address these limitations, field data-based modulus estimation techniques have gained prominence. These include dynamic tests such as the FWD, LWD, and APLT, which estimate stiffness by analyzing surface deflections or load-settlement responses under applied loads (White et al., 2018). These methods are increasingly favored for their ability to provide in-situ data that reflect field compaction, moisture content, and actual boundary conditions. Among them, the APLT has shown promise for evaluating the stiffness characteristics of base layers with or without stabilization, as it allows repeated loading sequences to simulate traffic-induced stress paths and permits integration with embedded sensors for simultaneous monitoring (White et al., 2018; White & Vennapusa, 2017).

In addition to multilayer stiffness assessments, localized stiffness characterization is crucial for detecting variations within pavement layers, especially in mechanically stabilized layers where geogrid placement may lead to depth-dependent behavior. Shear wave velocity (Vs) measurements obtained through BE Field sensors have been adopted to estimate small-strain stiffness in both laboratory and field applications (Byun & Tutumluer, 2017). These sensors provide high-resolution, localized data that can help quantify the influence of geogrid placement and interlock development over time. Because Vs is directly related to the elastic shear modulus and less sensitive to large-scale deformation (J.-S. Lee & Santamarina, 2005; Santamarina et al., 2001), BE testing complements deflection-based methods by providing insight into early-stage degradation and long-term stiffness evolution.

Advancements in data acquisition and sensor technologies have also enabled long-term monitoring of stiffness behavior under real-world loading and climatic conditions. The integration

of pressure cells, BE sensors, and moisture-temperature probes in full-scale test sections facilitates continuous tracking of stiffness evolution and provides empirical data for validating mechanistic models (Kang, 2023). These datasets are essential for capturing stress redistribution effects and understanding the role of geogrids in moderating seasonal and traffic-induced variability in base layer performance.

In summary, the characterization of pavement foundation stiffness has evolved from conventional laboratory testing toward integrated field-based and sensor-informed approaches. These tools are particularly critical when evaluating geogrid-stabilized systems, where localized confinement and enhanced particle interaction may lead to complex, spatially variable mechanical responses. A comprehensive assessment requires both global and local stiffness measurements that account for stress dependence, environmental effects, and stabilization mechanisms, forming the basis for improved design and long-term performance predictions.

2.4 Applications of BE Field Sensor and APLT

The mechanical behavior of pavement foundation materials under repeated loading is governed not only by their intrinsic properties, but also by environmental factors and construction practices. To evaluate this behavior in a realistic and quantifiable manner, researchers and practitioners have increasingly adopted in-situ and laboratory testing methods capable of capturing the evolving stiffness of unbound aggregates. Among these, BE Field sensor and APLT have gained recognition for their complementary roles in assessing both small-strain and operational-scale modulus characteristics.

BE testing is a nondestructive method used to determine the Vs of geomaterials, from which the small-strain shear modulus (G_{max}) can be inferred (Byun et al., 2019; Santamarina et al., 2001). In pavement applications, embedded BE sensors can be installed in laboratory specimens or in field test sections to monitor stiffness evolution over time. Because Vs reflects the speed at which shear waves propagate through a medium, it serves as a sensitive indicator of material structure, particle contact conditions, and confinement. This makes BE measurements particularly useful for assessing the effects of geogrid stabilization, which influences lateral restraint and aggregate interlock, especially in the vicinity of the stabilization layer (Byun et al., 2019).

In recent years, field-deployable BE sensors, as shown in Figure 2.1, have enabled researchers to measure shear wave velocities at multiple depths and locations within constructed pavement layers, thus providing valuable insights into the spatial and temporal variations in stiffness induced by environmental cycles or repeated traffic loading (Kang et al., 2021). These data have been instrumental in identifying the formation and persistence of an MSL in geogrid-stabilized base sections. Additionally, periodic BE testing has been used to quantify stiffness retention over freeze-thaw cycles and to isolate the influence of geogrid placement depth on small-strain behavior.

While BE testing offers high-resolution, local stiffness characterization at small strains, APLT provides a more global assessment of the load-deformation behavior of pavement layers under applied surface loads. The APLT device, as shown in Figure 2.2, applies a series of static and cyclic loads to a rigid plate while recording corresponding deflections with high precision (Husain et al., 2025; White & Vennapusa, 2017). Unlike traditional plate load tests, APLT is automated and allows for multiple loading-unloading cycles that more closely simulate traffic conditions. This enables the extraction of nonlinear modulus values change with loading and the evaluation of stress-dependent behavior.

The backcalculation of resilient modulus information from APLT data, typically performed through layered elastic analysis or finite element modeling, allows practitioners to evaluate effective composite stiffness values across pavement layers. When coupled with spatial sublayering and iterative parameter calibration, APLT results can be used to derive resilient modulus inputs for ME design tools, such as the AASHTOWare PMED. In geogrid-stabilized bases, APLT data have been used to demonstrate depth-dependent stiffness improvements, reflecting the confinement and load-spreading effects introduced by geogrids (Husain et al., 2025; White & Vennapusa, 2017).

Together, BE and APLT methods can provide a comprehensive understanding of pavement foundation behavior. BE testing captures localized changes in stiffness at very small strains, which are critical for understanding structural integrity and early-stage degradation. APLT, on the other hand, reflects system-level responses under operational loading ranges, making it a valuable tool for calibrating design inputs and validating structural models. When used in tandem, these methods enable multiscale evaluation of geogrid-stabilized systems, from particle-scale stabilization effects to aggregate-layer modulus enhancement and stress redistribution.

2.5 Summary of Previous Research and Identified Gaps

Extensive research over two decades has investigated the performance benefits of geogrid-stabilized unbound aggregate layers in pavement systems. Laboratory studies, full-scale tests, and numerical modeling show enhanced load distribution, reduced rutting, and improved stiffness under traffic loading. However, measuring, interpreting, and incorporating these benefits into design frameworks remains challenging. Previous experimental work suggests developing an MSL in geogrid-stabilized sections, characterized by increased lateral restraint, reduced vertical deformation, and altered shear stress distributions. These effects are more pronounced under repeated loading. Yet, current design practice relies on simplified modulus characterization or assuming no effect by neglecting geogrid stabilization influence or lateral restraint.

Testing methodologies include cyclic plate load testing, large-scale triaxial testing, and field measurements. These approaches are useful for comparative analysis but lack resolution to capture stress-dependent and spatially varying behaviors within the base layer. Laboratory specimens may not fully represent in-situ compaction, moisture variation, and field construction practices. Recent advancements in sensor-based techniques, such as BE Field sensors and APLT, offer new opportunities for in-situ

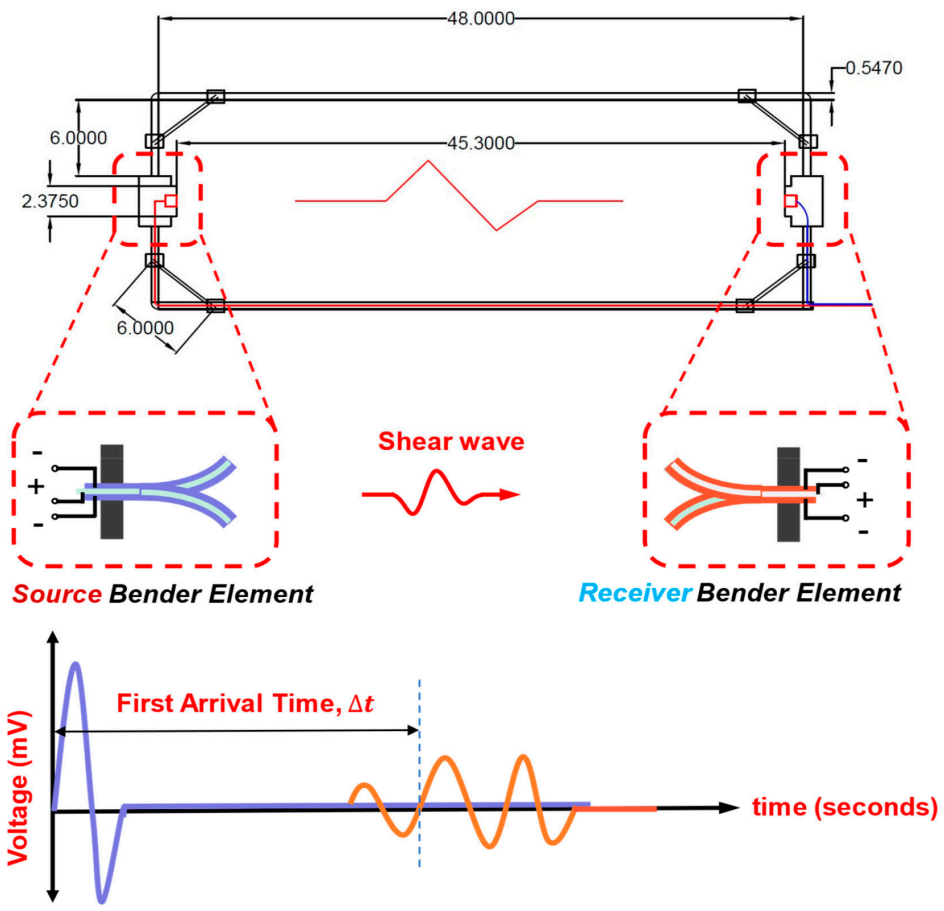

(a)

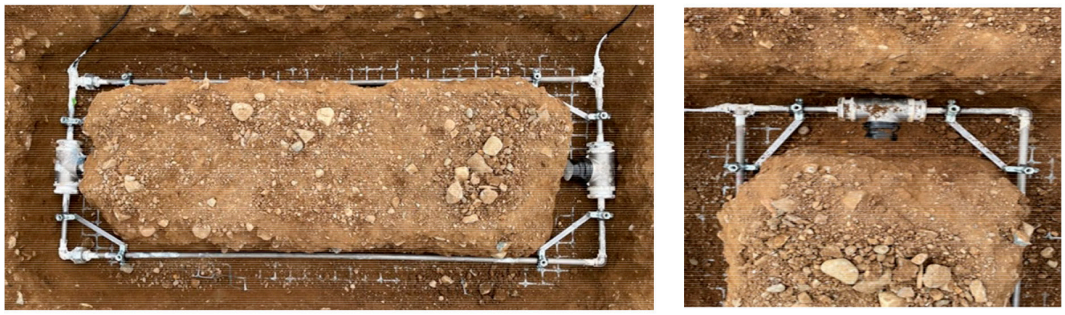

(b)

Figure 2.1 BE Field Sensor (a) Detailed Drawing of Sensor Showing a Characteristic Signal From Kang (2023) and Kang et al. (2021), and (b) Installed BE Field Sensor in the US 20 Reconstruction Project Pavement Test Section With Geogrid. Note: All measurements in inches (1 in. = 25.4 mm).

stiffness characterization under realistic loading conditions. These methods provide complementary perspectives on pavement response, with BE sensors capturing localized stiffness and APLT yielding operational-scale modulus values. However, the literature lacks integration between these data streams, limiting their utility in design calibration and model validation.

Another major gap involves translating geogrid-related performance enhancements into design inputs. Agencies

Figure 2.2 Photo Showing APLT Device (Insert: Load Plate and Linear Variable Differential Transformers [LVDTs]).

like INDOT assign uniform resilient modulus values to both geogrid-stabilized and nonstabilized bases in ME design procedures, neglecting observed stiffness gains and strain reductions. This practice results in conservative designs that may not fully capitalize on mechanical stabilization. While studies have investigated geogrid placement depth, type, and embedment conditions, there is no consensus on optimal configurations under different subgrade conditions or traffic loads. Long-term monitoring studies that evaluate performance under seasonal and traffic-induced variations are limited, especially those using high-frequency sensor measurements to capture stiffness and stress responses over time. In summary, while the literature confirms geogrid stabilization improves pavement foundation performance, current research lacks bridging the gap between experimental findings and practical design implementation. Key limitations include insufficient spatial resolution of stiffness characterization, limited integration of sensor-based data streams, lack of depth-specific modulus calibration, and underrepresentation of long-term field performance. Addressing these gaps is essential for adopting more refined and performance-based pavement design practices that reflect adequately structural contributions of geogrid-stabilized systems.

3. CONSTRUCTION OF PAVEMENT TEST SECTIONS

3.1 Overview of the US 20 Test Site in Elkhart County

This chapter presents the construction and instrumentation of full-scale pavement research sections developed along a reconstructed segment of US 20 in Elkhart County, Indiana. The objective of this test site was to generate high-fidelity field data that could be used to evaluate the structural response and mechanistic performance of geogrid-stabilized and unstabilized pavement foundations under realistic construction and service conditions. The site was designed to support both short-term and long-term monitoring efforts aimed at quantifying stress dependent stiffness behavior, vertical stress on subgrade, and the development of MSLs in geogrid-enhanced base courses.

The test sections were established within a larger highway reconstruction project, providing a unique opportunity to embed sensors and conduct field testing in an operational roadway subject to representative construction practices and vehicular loads. A total of three test sections were constructed: one control section without geogrid and two geogrid-stabilized sections with varying placement depths. Each section incorporated identical pavement structures except for the presence and location of geogrid stabilization within the aggregate base layer. The materials used, including the INDOT No. 53 dense-graded aggregate base and B-Borrow subgrade replacement, were selected to reflect typical INDOT practice and ensure compatibility with field instrumentation.

An integrated instrumentation plan was developed to support both immediate postconstruction testing and long-term performance monitoring. Embedded sensors included BE Field sensors for measuring local stiffness, earth pressure cells for capturing vertical stress on top of subgrade and DCP for characterizing stiffness and penetration resistance. The APLT device was employed to induce controlled loading sequences while capturing layered pavement response in conjunction with sensor measurements.

3.2 Pavement Structure and Geogrid Installation

The full-scale research test site was established on a reconstructed portion of US 20 in Elkhart County, Indiana, between the intersections with State Route 15 (SR 15) and County Road 21. This location was selected in collaboration with INDOT to facilitate embedded instrumentation and performance evaluation as part of a routine reconstruction effort. Incorporating the research into an active INDOT project allowed field testing and long-term monitoring to be carried out under representative construction and service conditions.

Several key considerations informed the selection of this site. First, the US 20 corridor is a major east–west freight route with substantial truck traffic, making it a suitable candidate for evaluating the stress-sensitive behavior of pavement foundation layers. According to INDOT's 2021 records, this segment of the highway carried an average annual daily traffic (AADT) of approximately 19,040 vehicles, with commercial trucks accounting for 26.9%. By 2024, updated counts recorded an AADT of 13,214 vehicles with 18% truck traffic, still representing substantial structural loading over the pavement foundation. These real-world traffic conditions establish a basis for interpreting load response and performance trends over time.

Second, the location provided geotechnical conditions of interest. During pavement reconstruction, the original swampy and peaty subgrade was excavated and replaced to a depth of approximately 15 ft using INDOT B-Borrow material. This sand sized uniform granular material was used across the test sections,

supporting consistent subgrade behavior that enhances the reliability of comparisons made between the control and geogrid-stabilized sections. These efforts to minimize variability also facilitated meaningful interpretation of DCP, LWD, and pressure cell data, which are further analyzed in Section 4.1 (Preliminary Site Characterization) and Section 4.2 (APLT Data Analysis).

As shown in Figure 3.1, the total research testbed length was approximately 750 ft (228.6 m), divided into three consecutive 250 ft (76.2 m)-long segments: a Control Section (CS), Geogrid Section 1 (GG1), and Geogrid Section 2 (GG2). Each section was constructed with the same pavement cross-section, consisting of a portland cement concrete (PCC) surface, hot-mix asphalt (HMA) drainage layer, HMA base course, a 12-in. (30.5-cm) subgrade treatment type 1C (INDOT No. 53 aggregate), and the engineered B-Borrow foundation. It should be noted that the data collected took place prior to the placement of HMA base. Therefore, for the purpose of this study, both unstabilized subgrade type IC and geogrid stabilized subgrade layers are referred to as "aggregate base" or simply "base" throughout the result discussion and interpretation portion of the report.

Detailed cross-sectional layouts and particle size distribution of No. 53 aggregate material for the three research sections are shown in Figure 3.2 and Figure 3.3 respectively, The only variation among the three sections was the placement of the biaxial geogrid: GG1 featured a single layer of biaxial geogrid at the base–subgrade interface, while GG2 incorporated geogrid at the mid-depth of the aggregate base. The control section did not include geogrid.

This testbed configuration supports multiple aspects of the study's experimental goals. It enabled the evaluation of base

Figure 3.1 Satellite Imagery Showing the Location of the Three Pavement Test Sections (Maps Data: © Google).

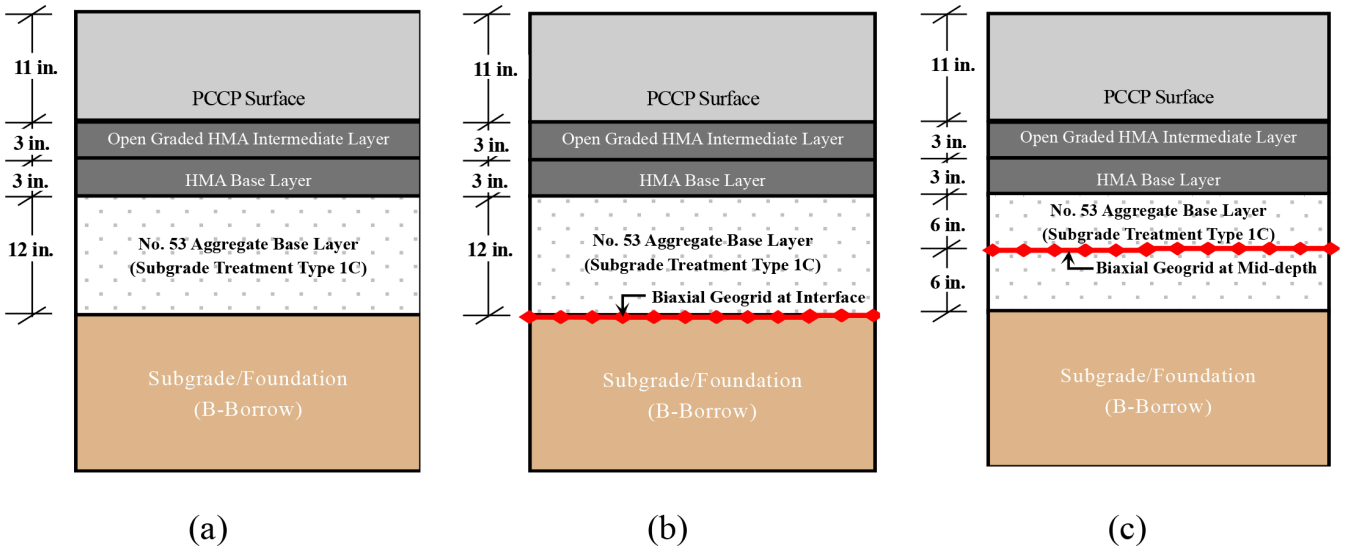

Figure 3.2 Layer Configurations for (a) CS, (b) GG1, and (c) GG2 (1 in. = 25.4 mm).

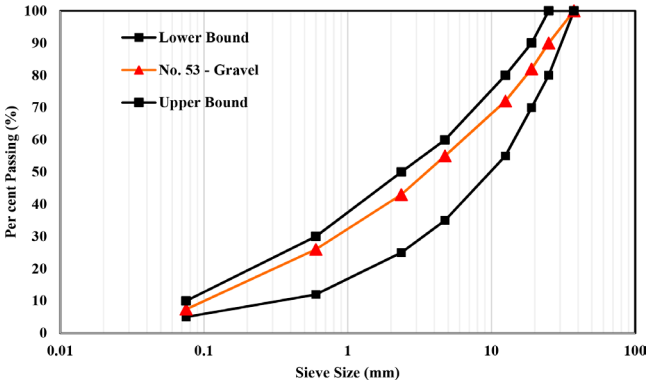

Figure 3.3 Particle Size Distribution of the Aggregate Material and the INDOT No. 53 Gradation Band Requirements (1 in. = 25.4 mm).

stiffness under different stabilization strategies using a suite of field instruments, including BE Field sensors, earth pressure cells, and in-situ characterization via DCP and LWD.

3.3 Instrumentation Plan and Sensor Deployment

A comprehensive instrumentation plan, as shown in Figure 3.4, was implemented across the three test sections, CS, GG1, and GG2, to measure in-situ pavement foundation responses during construction and long-term service conditions. The instrumentation strategy was developed to quantify both multilayer response and local mechanical behavior of the pavement layers, with specific focus on evaluating the stress dependent stiffness characteristics of geogrid-stabilized base aggregate layer and their effects on critical pavement response measures.

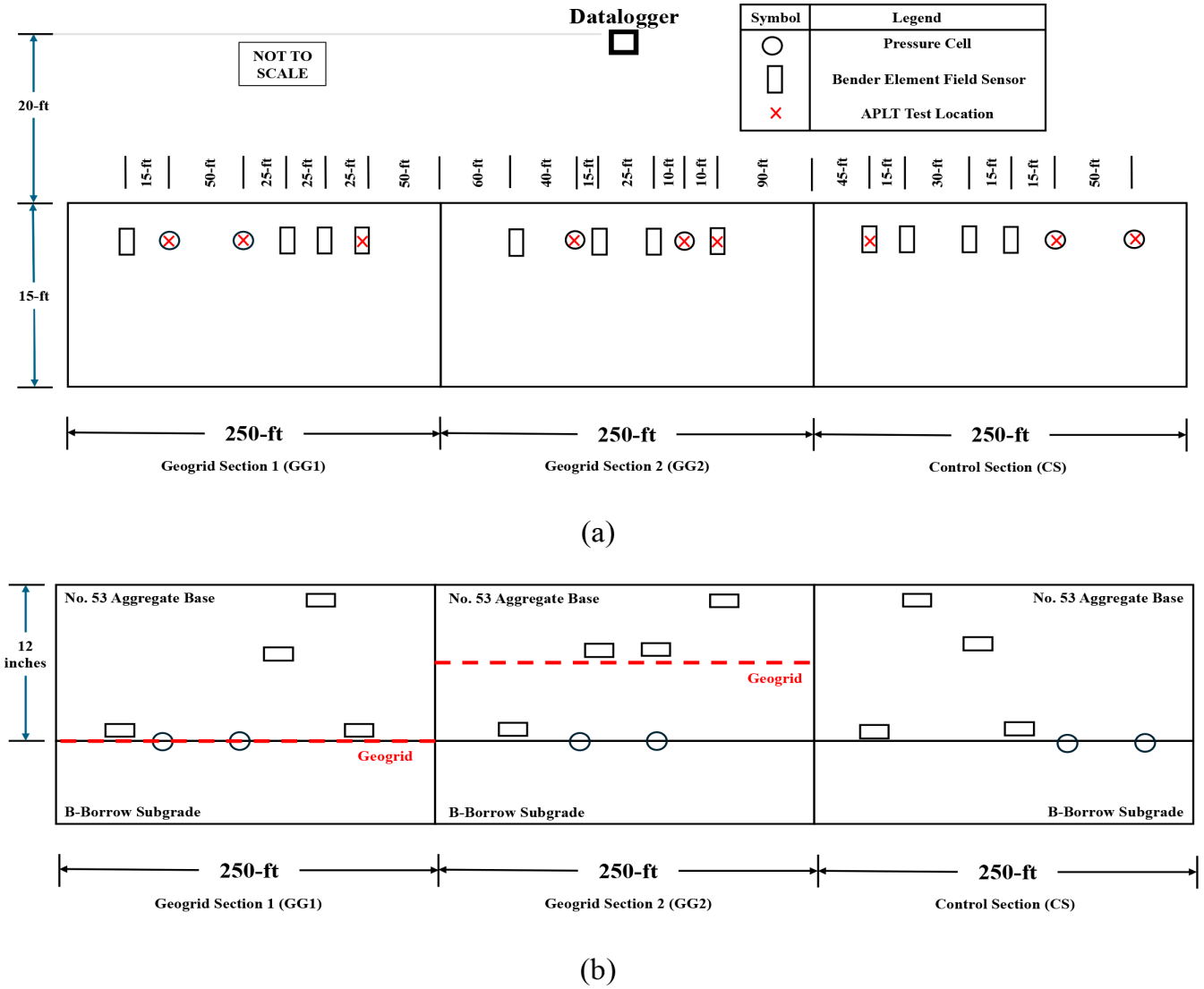

Figure 3.4 Locations of Installed Pressure Cells and BE Field Sensors and APLT Testing: (a) Plan View and (b) Longitudinal Cross-Section or Profile View (1 ft = 30.48 cm).

3.3.1 Instrumentation Objectives

The primary objectives of the instrumentation plan were to:

- Monitor vertical stress magnitudes on top of subgrade using embedded dynamic earth pressure cells during the APLT loading.
- Quantify the stiffness improvements in the aggregate base layer due to geogrid stabilization using BE Field sensors during the APLT loading.
- Monitor environmental factors, that is, moisture and temperature, to account for seasonal changes and climatic conditions.
- Support the interpretation of field modulus and stress sensitivity characterization of nonstabilized and geogrid stabilized aggregate layers and establish performance trends in relation to traffic and seasonal influences.
- Enable direct comparison between geogrid-stabilized and nonstabilized sections under identical pavement configurations.

3.3.2 Earth Pressure Cells

Two semiconductor-type earth pressure cells were installed in each test section at the interface between the base and subgrade layers. These sensors were designated to capture vertical stress (σ_v) as a function of applied loading during both short-term controlled loading via the APLT and monitoring-term traffic-induced loading.

- *APLT-Linked Acquisition*: High-frequency data (100 Hz) were collected during APLT stages to capture transient stress responses under repeated loading (see Section 4.2).
- *Long-Term Monitoring*: Low-frequency data (collected every 10 min) were logged over the full monitoring period between November 2023 through April 2025 to evaluate seasonal and traffic effects.

Sensor readings enabled evaluation of geogrid-induced stress distribution improvements and were colocated with BE sensors and surface test locations for integrated response interpretation. Figure 3.5 illustrates the earth pressure cell installation procedure adopted during the field instrumentation.

3.3.3 BE Field Sensors

A total of four BE field sensors were installed in each section. These sensors operate by transmitting and receiving shear waves through the aggregate base, enabling computation of Vs, a direct indicator of small-strain stiffness.

- In geogrid-stabilized sections (GG1 and GG2), two BE sensors were positioned adjacent to the geogrid layer to monitor local mechanical stabilization effects.
- One sensor was placed near the top of the base layer and another near the base–subgrade interface in all three sections to track stiffness gradients.
- In the control section, one sensor was specifically positioned at the base–subgrade interface to monitor potential long-term intermixing effects.

The installation of BE sensors immediately following aggregate compaction ensured that the data represented initial stiffness characteristics. These measurements are essential for assessing stress sensitivity and modulus enhancement ratios (introduced later in Section 4.5) and contributed to calibration of the sublayering approach discussed in Section 5.3.

3.3.4 Site Characterization

In addition to embedded instrumentation, the following characterization tests were colocated with sensor locations:

- DCP tests were performed adjacent to pressure cell locations to evaluate subgrade stiffness and penetration resistance. These measurements supported interpretation of pressure cell readings (see Section 4.1).
- LWD testing was performed in each section to evaluate immediate postcompaction modulus of the base layers. Both point deflection values and deflection basins were used to compare load distribution trends.

3.3.5 Data Logging and Integration

All instrumentation was connected to a centralized data acquisition via Campbell Scientific CR6 datalogger programmed for two modes of operation: (1) high-frequency event-based acquisition during APLT testing, and (2) long-term autonomous logging for seasonal and traffic analysis. All data were time-synchronized across sensors to allow interpretation of stress-strain behavior under variable field conditions. This integrated sensor

Figure 3.5 Earth Pressure Cell Installation Procedure. Left to Right: Marking Location for Each Sensor, Trench and Ensure Fit, Prepare a Uniform Base for the EPC With Mason Sand, Installing the Sensor and Covering With Subgrade Material. Finally, Each Sensor is Geo-Referenced.

Figure 3.6 BE Field Sensor Installation Procedure. From Left to Right: Mark Location of the Sensor, Prepare Trench, Install the Sensor Frame in Trench Ensuring Uniform Placement Depth, and Finally, fill Sensor and Cable Trenches.

framework enabled detailed mechanistic interpretation of pavement foundation response, forming the empirical basis for the results and calibration presented later in the report.

3.4 Description of Testing Protocols

This section outlines the field-testing protocols used to evaluate the stiffness and stress response characteristics of the pavement foundation layers constructed at the US 20 test site. The protocols were selected to ensure both depth-resolved and integrated characterization of the pavement base and subgrade layers. Embedded sensors, nondestructive surface tests, and load-deformation-based methodologies were combined to obtain a comprehensive understanding of pavement behavior under applied loading.

3.4.1 BE Field Sensor Setup

The BE Field sensors used in this study were embedded horizontally at various depths within the aggregate base layer in all three test sections. Each sensor consisted of a paired piezoceramic source and receiver encapsulated in waterproof housing. The source element generated shear waves through voltage-induced mechanical deformation, and the receiver recorded wave arrivals at high resolution. Sensor positions were carefully selected to capture gradients in shear wave velocity across the base layer. In the geogrid-stabilized sections, sensors were placed immediately above and below the geogrid layer to evaluate localized stiffness enhancement due to geogrid-induced confinement. In the control section, sensors were distributed at the top, mid-depth, and bottom of the base layer, including at the base–subgrade interface to detect any long-term material intermixing.

Field deployment was carried out immediately following base layer compaction, as shown in Figure 3.6, highlighting the BE field sensor installation procedure. After placement, each sensor was tested for signal clarity and continuity. Data were recorded intermittently using an oscilloscope-based acquisition system configured to capture waveforms over a burst period sufficient for clear shear wave identification. Shear wave velocity was computed using the known travel distance between the source and receiver and the measured time of wave arrival. These measurements provided direct estimates of small-strain stiffness and were later used to assess modulus enhancement and stiffness retention in the geogrid-stabilized layers.

3.4.2 APLT Procedure

APLT was used as a repeated load testing methodology to assess both resilient and permanent deformation characteristics of the base layers in all test sections. The APLT device applied a sequence of vertical stresses through a circular plate with a known footprint. A repeated haversine loading waveform was employed with loading levels ranging from 6 psi to 40 psi, representative of field-relevant stress conditions. Each load sequence was programmed to run through multiple cycles with prescribed durations and rest periods, typically 0.2 s of loading followed by a 0.8 s rest interval before next set of loading pulse is applied. Deflection sensors captured the vertical rebound and permanent deformation at the center of the load plate after each cycle. These values were then used to calculate composite resilient modulus. During selected APLT stages, BE field sensors and earth pressure cells were actuated simultaneously to capture synchronized stiffness and stress response data. This paired instrumentation approach allowed for direct interpretation of modulus evolution, stress transmission, and the formation of mechanically stabilized layers in geogrid-stabilized sections. Detailed multistress staging of APLT loading is tabulated in Table 3.1.

3.4.3 DCP and LWD Testing

A suite of nondestructive and penetration-based tests was conducted at key stages of construction to support interpretation of base and subgrade mechanical properties. The DCP test was used to evaluate the penetration resistance of the subgrade directly below each test section. Tests were conducted adjacent to embedded pressure cells to contextualize the stress response data. DCP readings also provided layer strength indices that

TABLE 3.1
Multi-Stress Sequence Applied During APLT Testing.

Stage No.	Number of Cycles, N	Repeated Vertical Stress, $\sigma_{repeated}$, psi (kPa)	Min. Vertical Stress, σ_{min}, psi (kPa)	Max. Vertical Stress, σ_{max}, psi (kPa)
Conditioning	500	13 (89.6)	2 (13.8)	15 (103.4)
1	100	4 (27.6)	2 (13.8)	6 (41.4)
2	100	8 (55.2)	2 (13.8)	10 (68.9)
3	150	13 (89.6)	2 (13.8)	15 (103.4)
4	200	18 (124.1)	2 (13.8)	20 (137.9)
5	250	28 (193.1)	2 (13.8)	30 (206.8)
6	250	38 (262.0)	2 (13.8)	40 (275.8)

assisted in identifying spatial variability in subgrade stiffness. The LWD test was performed after placement of each lift of base layer to evaluate postcompaction stiffness. The device used a falling weight to apply transient loads through a small circular plate, and the resulting deflections were recorded using a geophone. These deflection measurements were used to calculate modulus estimates and consistency in load distribution trends across sections.

4. RESEARCH FINDINGS

4.1 Preliminary Subgrade and Base Characterizations

Establishing baseline aggregate layer conditions is essential for interpreting the effects of geogrid stabilization and evaluating long-term pavement response. During and immediately after construction of the base layer, the pavement foundation layers were characterized with in-situ testing and sensor measurements. This section summarizes the results of DCP testing performed after construction.

Pavement aggregate layers for all three test sections, one control and two geogrid-stabilized, were constructed within two weeks during September 2023 and under consistent weather and site conditions without a rainfall event. INDOT No. 53 gravel aggregate material was used as the base material for the reconstruction project including research test sections. Per standard INDOT specifications, quality control (QC) was performed on site by INDOT engineering team using a Zorn LWD deflection device and a deflection threshold of 50 mils was not exceeded for each lift of the No. 53 aggregate layer. The entire 12-in. layer was constructed in four 3-in. lifts, and for QC, LWD drops were performed in three locations every 50 ft of section length.

DCP testing was conducted in each of the three pavement test sections following completion of base construction and sensor installation. Three soundings per section were performed at locations adjacent to sensor locations where APLT tests were performed. DCP data, therefore, could offer complementary exposition to APLT stiffness response data. The DCP results, presented in Figure 4.1, provide depth-profile of penetration resistance based on the number of blows per unit depth of DCP penetration. A lower penetration index (PI; in in./blow or mm/blow) reflects stiffer materials, while a higher PI indicates reduced resistance.

For this study, average PI values were calculated separately for the full depth of the base layer and the upper 12 in. (30.5 cm) of the subgrade. The geogrid-stabilized sections (sections GG1 and GG2) consistently exhibited lower PI values within the aggregate base layer compared to control, indicating improved penetration resistance near and above the geogrid interface. These trends suggest the presence of an MSL, where aggregate interlock and lateral restraint contribute to increased stiffness. This behavior is consistent with past studies on geogrid-stabilized layers (Al-Qadi et al., 2006; Kwon & Tutumluer, 2009).

As shown in Figure 4.2, the average PI for the aggregate base layer was 0.16 in./blow (4.0 mm/blow) in the control section, compared to 0.11 in./blow (2.8 mm/blow) and 0.12 in./blow (3.1 mm/blow) in GG1 and GG2, respectively. Subgrade PI values also followed a similar trend, with slightly lower indices in the stabilized sections. The similarity between geogrid sections confirms consistent construction and geogrid performance across replicates. However, a softer subgrade in control could skew the APLT measurements, thereby impeding the ability to isolate geogrid benefits.

Therefore, DCP results support qualitative assessment of relative stiffness and confirm enhanced resistance in stabilized layers. They do not directly provide input parameters for mechanistic analysis. Further analysis using APLT and BE sensor data is presented in the following sections to evaluate stress dependent behavior and small-strain stiffness characteristics to directly quantify geogrid benefits.

4.2 APLT and Pressure Cell Measurements

The APLT was employed to evaluate the geogrid-aggregate composite layer repeated load response in all three instrumented road test sections. APLT direct measurements include target stress applied using a hydraulic loading actuator and surface deflections measured using linear variable differential transformers (LVDTs). During APLT loading, Earth Pressure Cell (EPC) data were collected to provide insights into vertical stress transmission through the pavement layers on the subgrade. Together, these measurements offer a better understanding of pavement foundation behavior and influence of geogrid stabilization.

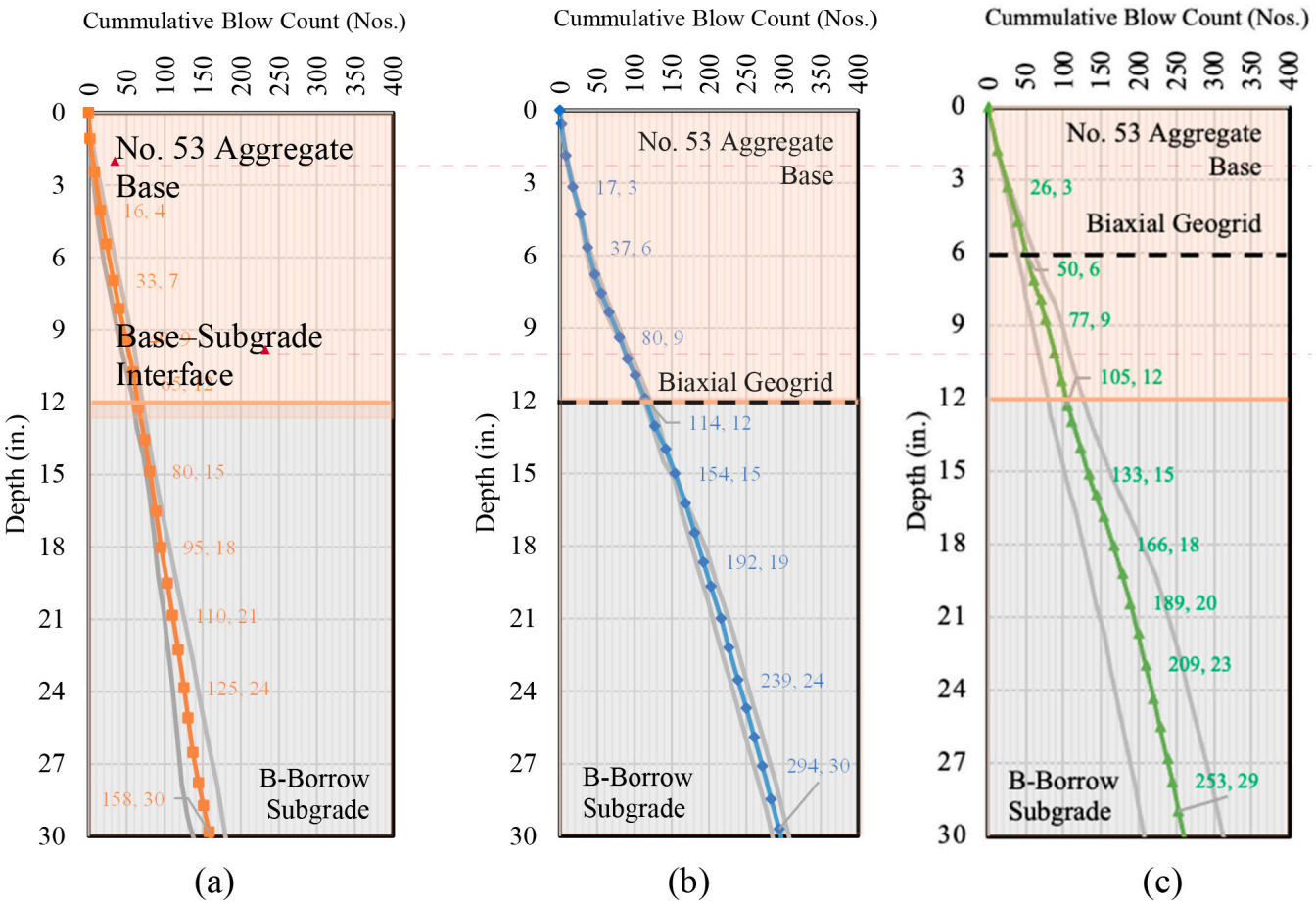

Figure 4.1 DCP Blow Count Profiles: (a) CS, (b) GG1, and (c) GG2 (1 in. = 25.4 mm).

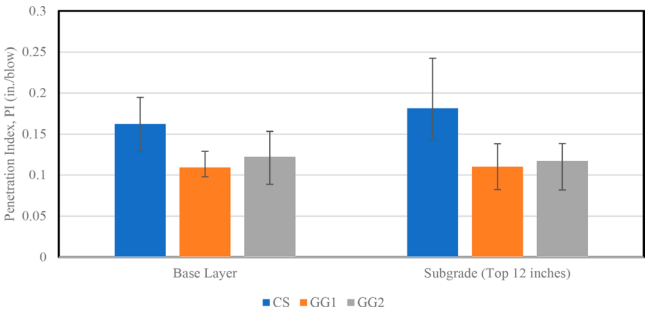

Figure 4.2 Average Penetration Indices for the Base and Subgrade Layers in the Three Sections (1 in. = 25.4 mm).

The APLT loading was applied using an 18-in.-diameter rigid plate centered over embedded sensor locations in successive increments to simulate standard laboratory repeated load testing protocols, with multiple load repetitions in each step. Deflection beneath the plate was measured using displacement sensors mounted at the plate center. Surface deflection data were then used to backcalculate the composite resilient modulus of the pavement foundation using the Boussinesq equation, as shown below in Equation 4.1, assuming one-layer elastic and homogeneous support condition.

$$\delta_r = \left(1-\nu_1^2\right)\sigma_0 rf\left[\frac{1}{M_{R(sg)}\sqrt{1+\left(\left(\frac{h}{r}\right)\left(\sqrt[3]{\frac{M_{R(base)}\left(1-\nu_1^2\right)}{M_{R(sg)}\left(1-\nu_2^2\right)}}\right)^2}} + \frac{1-\left(\frac{1}{\sqrt{1+\left(\frac{h}{r}\right)^2}}\right)}{M_{r(base)}}\right]$$

Equation 4.1

where ν_1 *and* ν_2 are Poisson's ratios for the base and subgrade, σ_0 is the applied stress, h is the thickness of the base layer,

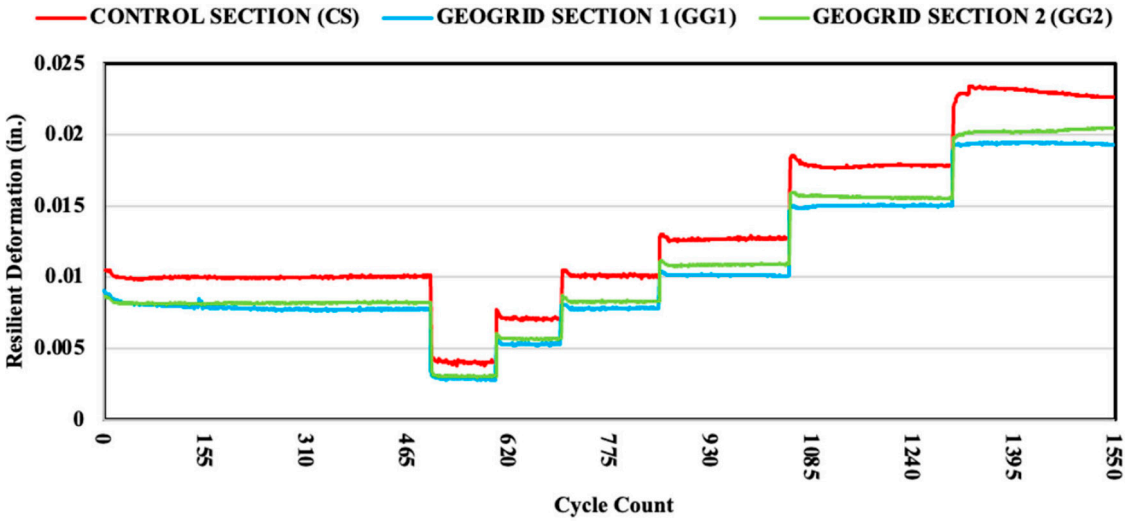

Figure 4.3 Resilient Deformation (δ_r) Data Trends Collected With APLT (1 in. = 25.4 mm).

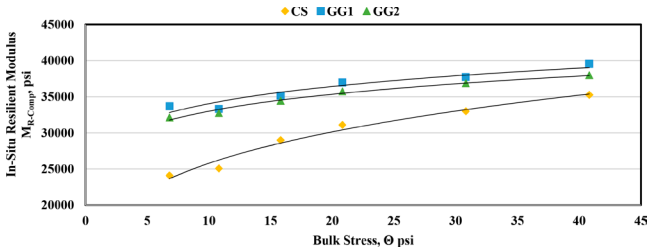

Figure 4.4 In-Situ Composite Resilient Modulus ($M_{R\text{-}Comp}$) for the Three Sections From APLT (1 psi = 6.9 kPa).

r is the plate radius, and *f* is the shape factor. For this study, a shape factor of 8/3 was selected as recommended by (White & Vennapusa, 2017). Figure 4.3 presents rebound deflection measured on top of the loading plate during the multistress staging of the APLT device. The control section exhibited greater deflections at comparable load levels relative to the geogrid-stabilized sections, indicating a reduced stiffness response later quantified as lower composite resilient modulus. Modulus estimates derived from these deflections, therefore, confirmed enhanced stiffness in the stabilized sections, particularly under higher load steps. Across all tests, the geogrid sections demonstrated composite resilient modulus values approximately 20–35% higher than the control section, as illustrated in Figure 4.4.

The enhanced stiffness response observed in the geogrid sections is attributed to the formation of an MSL, where lateral confinement improves aggregate load distribution and reduces vertical deformation. The increase in composite modulus was most pronounced during initial load steps and stabilized with increasing load repetitions, suggesting effective load transfer and minimized layer disruption in stabilized zones. To confirm this, vertical stress on top of subgrade was evaluated using EPCs embedded at the interface between the base and subgrade. EPCs recorded real-time vertical stress during each APLT load step. Figure 4.5 shows the measured stress attenuation through the pavement layers. In the control section, EPCs consistently recorded higher subgrade stress magnitudes compared to the geogrid-stabilized sections. This indicates a larger proportion of applied surface stress being transmitted downward in the absence of geogrid, whereas the geogrid sections demonstrated more effective lateral dispersion of stress.

On average, peak vertical stresses at the subgrade interface in the control section were 20–25% higher than those recorded beneath the geogrid sections under equivalent surface loads. This reduction in stress transmission corroborates the hypothesis that geogrid stabilization improves aggregate layer stiffness mitigating critical pavement response on top of subgrade, potentially reducing long-term deformation accumulation and resulting in rutting distress development.

Collectively, the APLT and EPC results confirm that geogrid stabilization enhances the load-bearing capacity of the pavement foundation by increasing overall stiffness and reducing vertical stress transferred to underlying subgrade soil. These improvements are directly linked to performance benefits in terms of rutting resistance and structural lifespan, which are explored in more detail in subsequent sections. It should be noted that the contribution of the subgrade layer in composite layer measurements is significant, therefore, the benefits established from APLT-EPC measurements should be conservatively treated in design. In accordance, the following section reports on the findings from the embedded BE Field sensor measurements for a direct quantification of geogrid benefits.

4.3 Local Stiffness Trends from BE Field Sensors

BE Field sensors were embedded within the aggregate base layers of the test sections to measure Vs over time. These measurements allow estimation of G_{max}, providing a sensitive indicator of local stiffness changes in response to compaction, environmental effects, and traffic loading. Compared to surface testing methods,

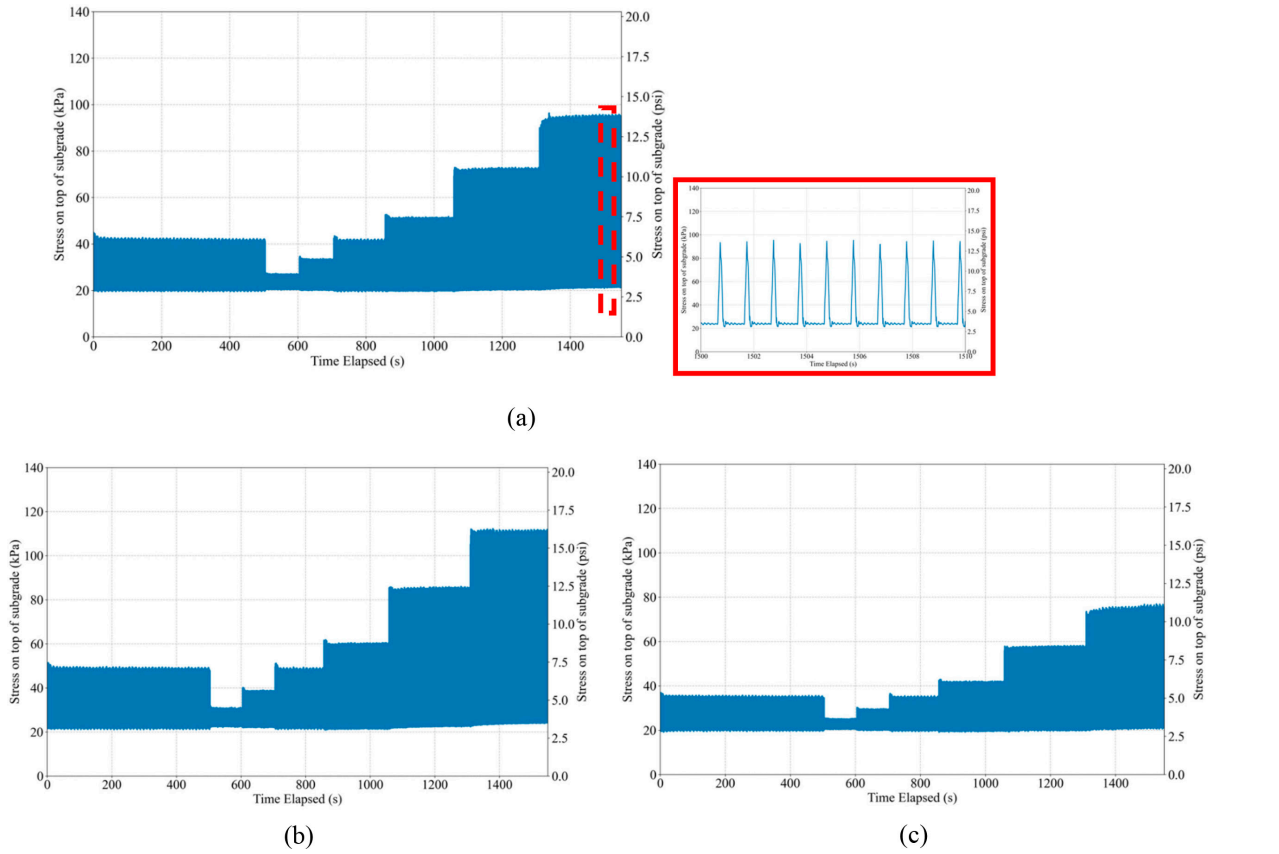

Figure 4.5 Pressure cell Measurements Under APLT Repeated Loading for (a) CS With Insert Showing Repeated Load Pulses Measured at Subgrade, (b) GG1, and (c) GG2.

BE sensors enable continuous, localized monitoring of stiffness evolution at specific depths with minimal disturbance.

Sensors were installed at two to three depths within each section, that is, near the top of base, mid-depth, and at the base–subgrade interface. Data were collected periodically using a custom field acquisition protocol, ensuring consistent excitation and signal interpretation over the study duration. The Vs was calculated from the first-arrival travel time between transmitter and receiver pairs, with known offset distances.

Subsequent sections present the interpretation of stress dependent stiffness behavior in the pavement foundation layers based on composite surface response and localized Vs measurements. The analysis draws on paired data obtained from the APLT device and the embedded BE Field sensors. While APLT provides information on composite stiffness under increasing static and repeated loading, BE sensors offer depth-specific stiffness characterizations through the measurement of shear wave velocity. This paired testing methodology was specifically designed to address limitations in surface testing and to directly quantify the MSL influence zone associated with geogrid stabilization.

4.3.1 Baseline BE Shear Wave Velocity Measurements

Immediately following construction and compaction of the base layers, BE sensors embedded at three depths were activated to measure baseline shear wave velocities across all test sections. These measurements were taken prior to the placement of HMA and Portland Cement Concrete Pavement (PCCP) layers, or application of any surface loading to capture the as-constructed stiffness profile. As shown in Figure 4.6, the mid-depth Vs measurements made in the control section were slightly lower than those in the geogrid-stabilized sections. All sections, however, exhibited similar Vs values, attributable to the lack of composite geogrid-aggregate interlock mobilization after construction under no stress conditions.

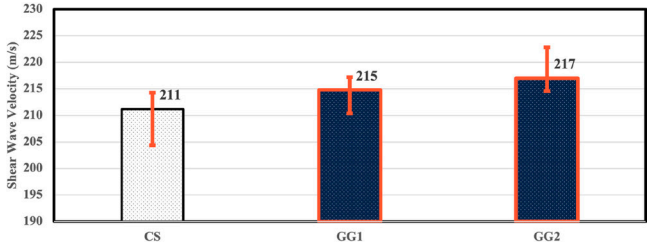

Figure 4.6 Shear Wave Velocities (V_S) Measured at the Mid-Depth of the Aggregate Layer in Three Test Sections (1 in./s = 0.0254 m/s).

4.3.2 *Paired Testing Under APLT Loading*

To evaluate the effect of APLT loading on stiffness development in the road test sections, a paired testing protocol was employed. APLT loading was conducted directly above embedded BE sensors, and shear wave velocity measurements were taken under two defined target stress levels:

- **13 psi (90 kPa)** representing low stress/conditioning load
- **38 psi (262 kPa)** simulating high service-level repeated loading

For each loading stage, BE signals were recorded and filtered to isolate the first-arrival shear wave. Time-of-arrival calculations were performed to derive Vs values under load. To quantify the stiffness improvement due to geogrid inclusion, a BE enhancement ratio (ER_{BE}) can be defined as:

$$ER_{BE} = \frac{V_{s,geogrid}}{V_{(s,control)}} \qquad \text{Equation 4.2}$$

At the 13-psi conditioning stress, both geogrid sections exhibited ER_{BE} values near 1.11, indicating an 11% increase in local stiffness relative to the control. At the 38-psi repeated load level, ER_{BE} decreased to approximately 1.07, reflecting a well-documented unbound aggregate behavior, that is, as applied stress increases, all materials experience stiffness gain, reducing the relative difference between geogrid-stabilized and non-stabilized sections. Figure 4.7 summarizes direct stiffness measurements across both stress levels under repeated loading.

These results confirm that geogrids improve local stiffness most effectively under low to moderate loads and that its relative effect diminishes as aggregate layers experience higher stress. It should be noted that the typical field stress conditions expected are significant below the APLT applied target stress levels. Additionally, the sustained advantage in Vs even under high load highlights the role of the geogrid in forming a structurally resilient MSL.

4.3.3 *Stress–Modulus Trends from APLT and BE Measurements*

Composite modulus values backcalculated from APLT data also increased with applied stress in all sections, confirming the stress dependent nature of foundation stiffness. However, the geogrid-stabilized sections consistently demonstrated higher initial modulus and a more stable modulus progression with load compared to the control. These trends, shown in Figure 4.4, reflects reduced sensitivity to applied stress, consistent with the confinement benefit observed in BE data. When interpreted together, the APLT and BE results demonstrate that:

- Geogrid-stabilized layers have higher initial stiffness, both at the surface and locally at a depth near the geogrid.
- Stress dependent stiffness changes are less pronounced in geogrid sections, resulting in reduced bulk stress sensitivity.
- BE sensors effectively capture geogrid-induced improvements in local stiffness and their evolution under loading.

The findings underscore the importance of integrating both composite and local measurements to capture the full structural benefit of geogrid stabilization. The multilayered stiffness response observed here reinforces the concept of an MSL and supports its consideration in mechanistic design frameworks.

4.4 Seasonal and Traffic-Induced Stiffness Variations

The velocity profiles with depth are presented in Figure 4.8, illustrating a clear localized enhancement in stiffness at or near the geogrid placement depth in both GG1 and GG2. These measurements were made after the placement of HMA and PCCP layer in November 2023. The development of MSL can be ascribed to in-situ static loading due to overburden, and initial shakedown during construction traffic movement along with moisture reduction postconstruction. The measurements confirm and demonstrate the capability of BE sensors to capture geogrid-induced enhancements within the internal aggregate layer structure.

The long-term behavior of unbound aggregate layers is influenced by seasonal moisture-temperature cycles and cumulative traffic loading. These external factors alter both stress transmission and stiffness within pavement foundations, and their combined effects can accelerate performance degradation, particularly in control sections. For geogrid-stabilized systems, it is critical to understand how initially observed benefits evolve under field conditions. This section presents findings from an extended in-situ monitoring program designed to assess these effects through integrated sensor data collected from the US 20 highway reconstruction project in Elkhart County, Indiana.

Embedded instrumentation included EPCs at the base–subgrade interface and BE Field sensors within the base layer. The goal was to evaluate the impact of traffic and environmental cycles, particularly

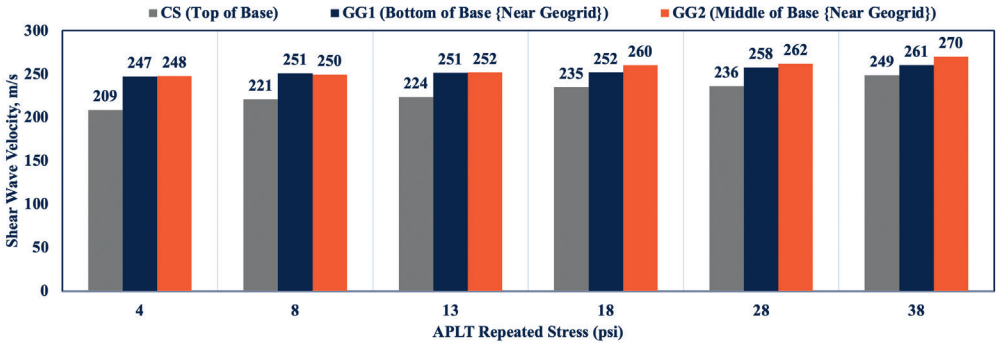

Figure 4.7 Summary of Paired APLT–BE Measurements Under Repeated Loading (1 in./s = 0.0254 m/s; 1 psi = 6.9 kPa).

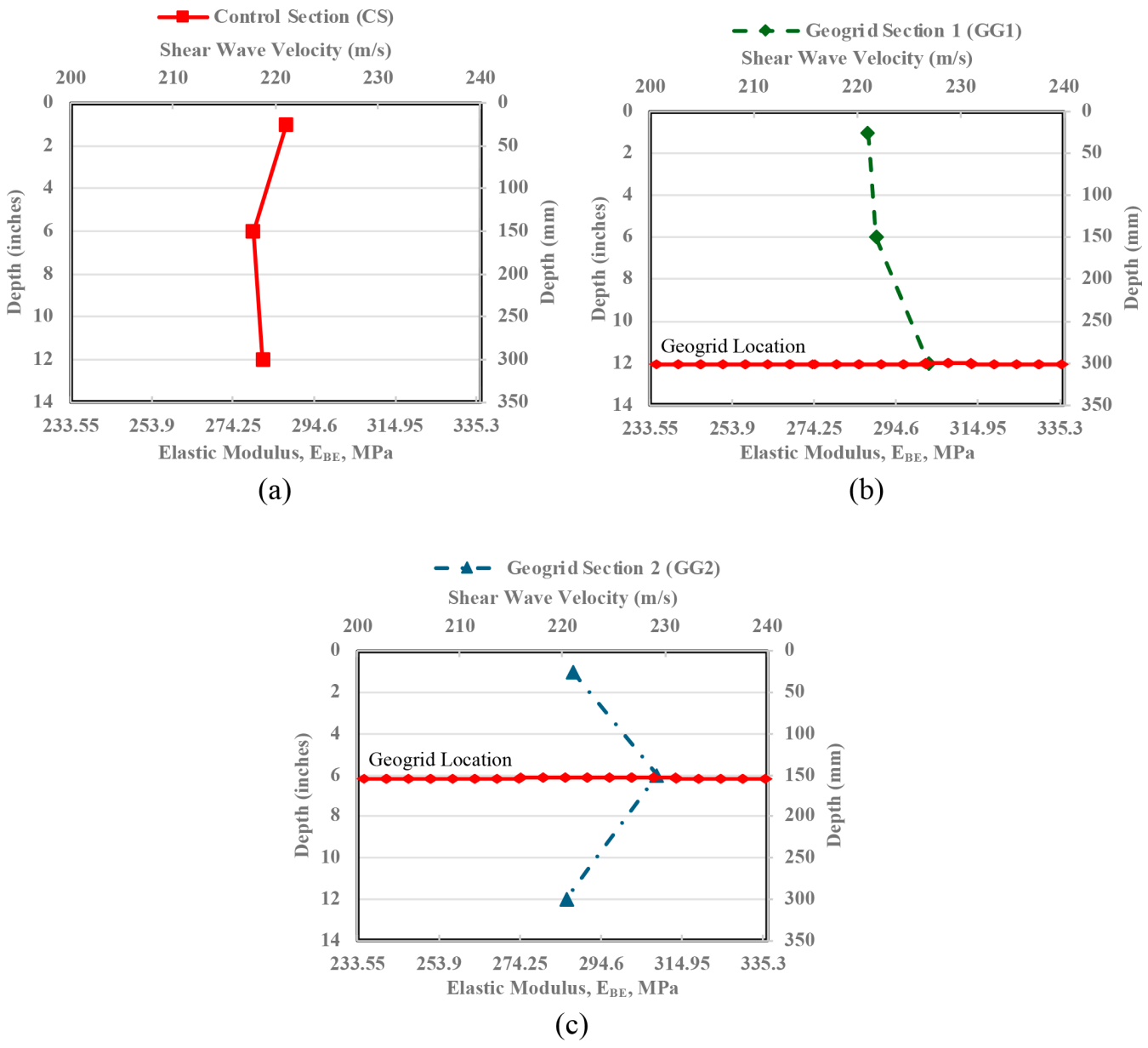

Figure 4.8 BE Shear Wave Velocity Profiles for (a) CS, (b) GG1, and (c) GG2.

freeze-thaw and wet-dry transitions, on stress attenuation and stiffness retention. Performance was assessed across a control section and two geogrid-stabilized sections (GG1 and GG2), the latter differing by geogrid placement depth.

4.4.1 EPC Observations Under Seasonal and Traffic Loading

EPCs provided continuous profiles of subgrade stress. As shown in Figure 4.9, stress levels were initially low across all sections during winter due to subgrade stiffening under frozen conditions. However, during spring thaw, as subgrade materials became more compliant, stress levels converged across sections, temporarily reducing the differential benefit of geogrid stabilization.

After the roadway opened to traffic in June 2024, divergence in subgrade stress levels emerged. GG2 consistently exhibited the lowest vertical stress transmission, followed by GG1, with the CS transmitting the highest stress. These differences became most evident during summer and early fall, when higher temperatures and increased subgrade moisture made load distribution more critical. Figure 4.10 illustrates monthly subgrade stress variation, showing clear performance stratification: GG2 < GG1 < CS.

Stress levels reconverged in the following winter months due to temperature-induced stiffening of the subgrade. However, the ranking persisted during transitional periods, reaffirming the ability of mid-depth geogrid placement (GG2) to attenuate subgrade stress more effectively.

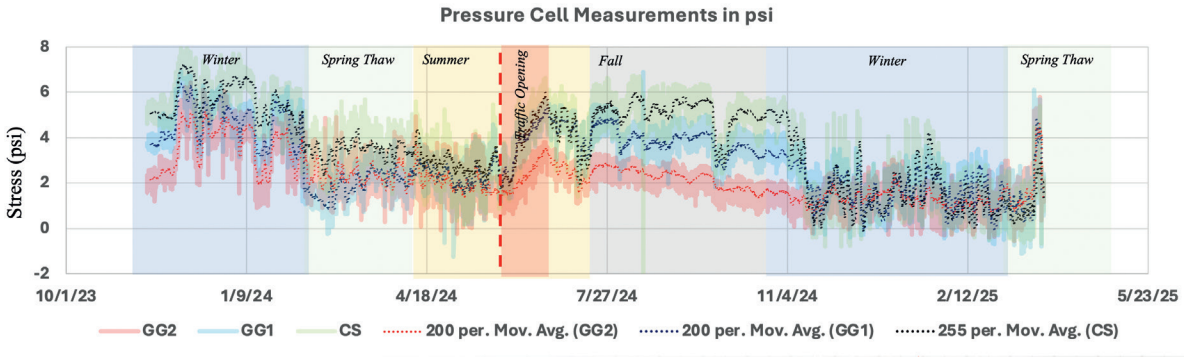

Figure 4.9 Fluctuations on Top of Subgrade Stress Levels Over Time During the Extended Road Test Study Period, as Recorded by Earth Pressure Cells.

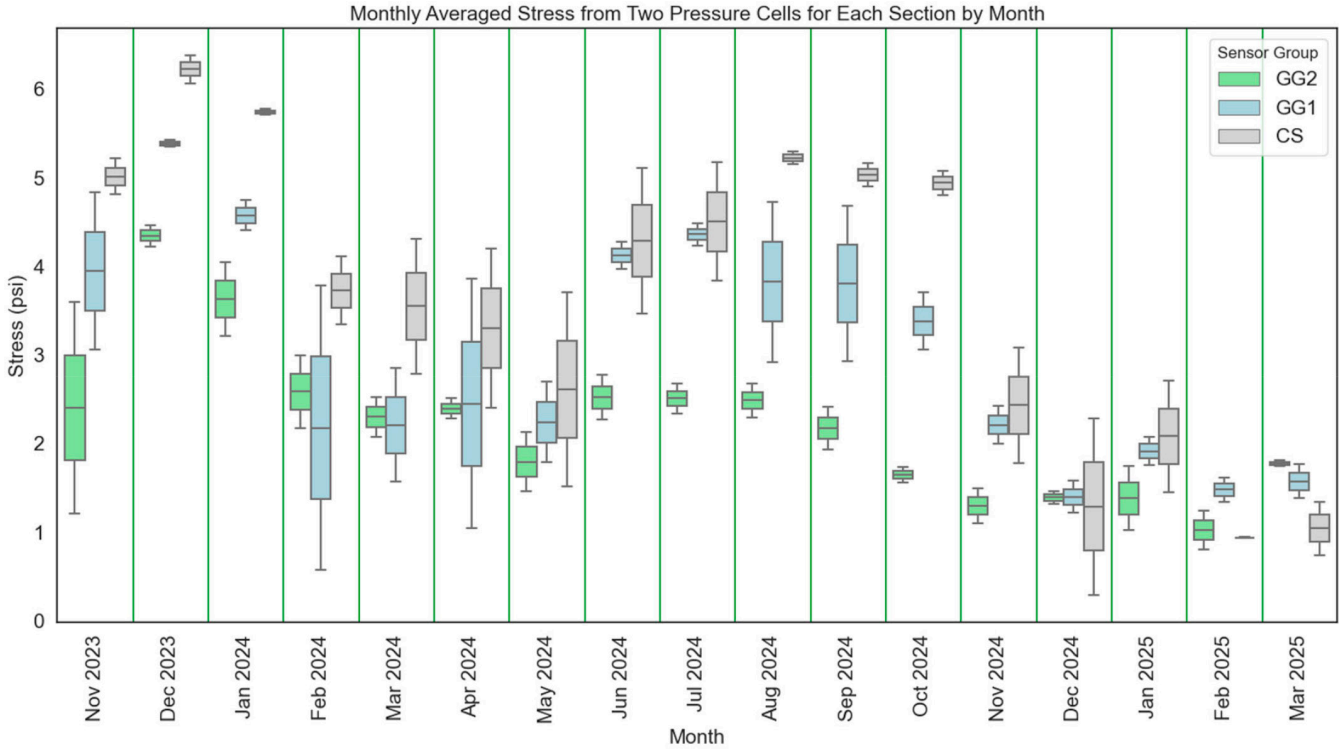

Figure 4.10 Boxplot Showing the Differences Emerging in Monthly Top of Subgrade Stress Averages as Measured With Earth Pressure Cells Over the Extended Study Period.

4.4.2 BE Field Sensor Trends in Stiffness Evolution

Periodic Vs measurements provided insights into base layer stiffness evolution. Measurements were taken postconstruction and then at key seasonal milestones: pretraffic, posttraffic, late summer, and postwinter. As shown in Figure 4.11, both GG1 and GG2 retained or increased their Vs values over time, indicating preserved or improved small-strain stiffness. In contrast, the control section exhibited a steady decline in Vs, suggesting degradation due to environmental cycling and traffic loading in the absence of lateral restraint. GG2 showed the most pronounced gain in stiffness, consistent with its reduced subgrade stress and better load distribution. Further, the differences in stiffness retention were amplified after the combined seasonal and traffic effects were experienced in March 2025. During this time, relatively higher ambient temperatures and increased traffic movement caused further reduction in the control section subgrade support leading to a reduced layer integrity and performance. Meanwhile, the GG1 and GG2 sections experienced significant modulus retention and recovery owing to the presence and functionality of MSL.

These Vs trends confirm that geogrid stabilization, particularly at mid-depth—a critical location from pavement design input perspective, supports the long-term mechanical integrity of the aggregate base layer, even under repeated environmental and traffic stresses.

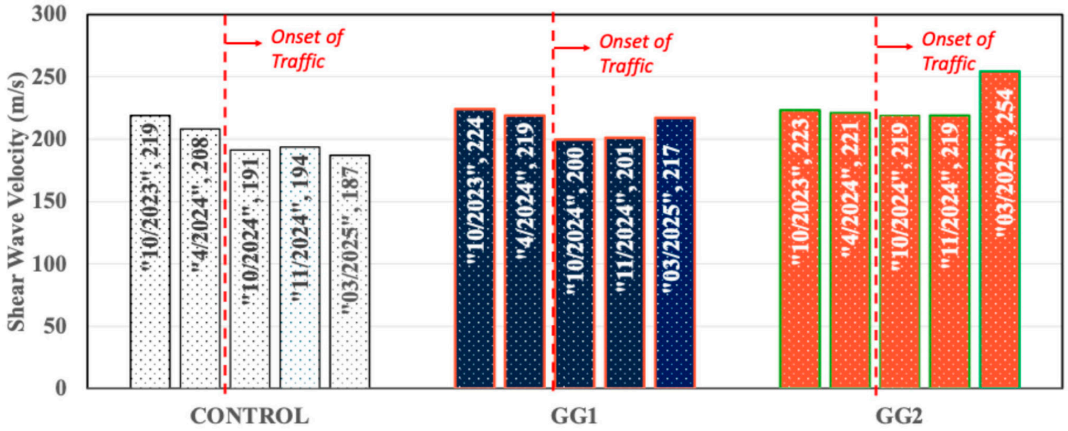

Figure 4.11 Vs Measurements From the Three Pavement Test Sections Over the Extended Study Period.

4.4.3 Interpretation of Combined Sensor Data

The combined analysis of EPC and BE sensor data for various stress states and over an extended time offers a holistic picture of pavement foundation performance. The concurrent reduction in subgrade stress and retention (or gain to a certain degree) in Vs measurements in geogrid sections confirm the formation and retention of an MSL, which plays a critical role during vulnerable periods such as spring thaw, when subgrade support weakens and nonstabilized systems are most susceptible to stress amplification and deformation leading to distress development.

Data from GG2 demonstrated that placement of the geogrid at mid-depth was more effective than subgrade-near installation (GG1) in enhancing base layer stiffness and attenuating stress transmission to subgrade. However, GG1 performed at par with GG2 in terms of modulus retention. These findings support a design overhaul for geogrid stabilization considering initial and long-term performance gains under variable field conditions.

4.5 Summary of Observations

This chapter presented the results of a comprehensive field investigation designed to evaluate the structural behavior of unbound aggregate base layers with and without geogrid stabilization. The findings are based on in-situ testing and continuous instrumentation data collected from three instrumented pavement sections constructed as part of the US 20 highway reconstruction project in Elkhart County, Indiana. Data were obtained using DCP soundings, APLT, BE Field sensors, and EPCs over an extended monitoring period. The following key observations were made from the analysis:

- Uniformity in Construction Conditions: Baseline DCP testing confirmed that all three sections were constructed over subgrade soils of comparable stiffness. This uniformity in foundation conditions provides confidence that performance differences observed across sections are attributable to the presence and configuration of the geogrid stabilization.
- Enhanced Composite Modulus from Surface Testing: Composite modulus values backcalculated from APLT loading demonstrated that geogrid-stabilized sections exhibited increased stiffness relative to the control section. This enhancement was most evident during initial load stages and was sustained across repeated loading cycles.
- Depth-Specific Stiffness Improvement: BE sensor measurements indicated higher shear wave velocities in the geogrid-stabilized sections, particularly at and near the geogrid elevation. These results confirm the formation of an MSL characterized by improved particle interlock and lateral restraint.
- Stress-Dependent Stiffness Behavior: Paired APLT–BE testing under incremental loading showed that while all sections exhibited increasing stiffness with stress, the geogrid-stabilized sections demonstrated higher initial stiffness and reduced stress sensitivity, suggesting a more resilient structural response.
- Attenuation of Subgrade Stress under Seasonal and Traffic Loading: Long-term EPC data revealed that geogrid-stabilized sections, and especially the section with mid-depth placement (GG2), consistently transmitted lower vertical stresses to the subgrade compared to the control section. These benefits were most pronounced during periods of increased subgrade vulnerability, such as spring thaw and post-rainfall softening events.
- Preservation of Stiffness over Time: Periodic BE measurements indicated that the control section experienced a decline in small-strain stiffness over the monitoring period. In contrast, both geogrid-stabilized sections maintained or slightly improved their stiffness characteristics, supporting the role of geogrid in promoting long-term mechanical stability.
- Influence of Geogrid Placement Depth: The section with mid-depth geogrid placement (GG2) consistently outperformed both the shallow-placement (GG1) and control sections in terms of stress attenuation and stiffness retention. However, both geogrid placement strategies prevented modulus degradation observed in control section. This finding highlights the importance of optimizing geogrid location within the base layer to achieve maximum performance benefit.

Collectively, these observations demonstrate that geogrid stabilization contributes to both immediate and sustained improvements in the mechanical behavior of aggregate base layers. The integration of high-resolution sensor data has

enabled a mechanistic interpretation of performance trends under realistic environmental and traffic loading conditions. These findings provide critical empirical support for the use of geogrid-stabilized bases in ME pavement design and lay the groundwork for the development of practical design recommendations.

5. IMPLEMENTATION OF RESEARCH FINDINGS INTO INDOT PAVEMENT DESIGN PRACTICE

ME pavement design relies on accurate characterization of pavement foundation materials, particularly the resilient modulus of unbound aggregate base layers. However, current design procedures often treat geogrid-stabilized and non-stabilized bases as equivalent, typically assigning a fixed modulus value regardless of geogrids. This approach overlooks the stiffness enhancement and stress distribution benefits introduced by geogrid inclusion.

Field testing conducted in this study, including APLT, BE shear wave velocity measurements, and pressure cell data, revealed both global and localized stiffness improvements in geogrid-stabilized sections. To translate these observations into design inputs, a modeling framework was established using the C-FLEX finite element program, developed for the US Army Corps of Engineers (Luo et al., 2021) to predict pavement responses. The C-FLEX analysis incorporates stress dependent behavior, sublayer discretization, and adjustment of Mechanistic-Empirical Pavement Design Guide (MEPDG) resilient modulus parameters to simulate the effects of mechanical stabilization.

This chapter presents the modeling configuration, parameter calibration procedures, validation using field measurements, and a parametric study exploring the influence of geogrid placement and pavement structure on subgrade response. The outcomes provide a pathway for incorporating geogrid-related benefits into pavement design through adjusted resilient modulus model parameter inputs or benefit ratios.

5.1 Modeling Framework and Objectives

The primary objective of the modeling effort was to quantify the stiffness enhancements provided by geogrid stabilization and to establish a practical methodology for incorporating these enhancements into ME pavement design procedures. Field testing results, including APLT-derived deflections and BE sensor shear wave velocity measurements, revealed that geogrid inclusion modifies both the magnitude and stress sensitivity of resilient modulus behavior within the aggregate base layer. However, to utilize these findings in design practice, a structured modeling framework is needed to translate observed in-situ responses into input parameters.

To address this need, a sublayering-based finite element modeling approach was developed using the C-FLEX program, a nonlinear layered elastic analysis tool capable of representing stress dependent, cross-anisotropic aggregate behavior (Luo et al., 2021). The model was configured to reflect the geometry, layer thicknesses, and material characteristics of the instrumented test sections constructed along US 20, with particular focus on capturing the mechanical effects of geogrid placement at different depths.

The framework was designed to support the following technical objectives:

- Simulate the formation of an MSL through depth-dependent modulus adjustment within the aggregate base.
- Calibrate the resilient modulus model parameters (k_1, k_2, k_3) for unbound layers based on backcalculated APLT field data.
- Apply localized modulus adjustment factors to reflect geogrid-induced confinement and stress redistribution.
- Validate model predictions using in-situ sensor data, including BE-measured shear wave velocities and pressure cell-derived subgrade stress.
- Quantify geogrid performance benefits using subgrade strain metrics and compute corresponding benefit ratios relative to control conditions.

This modeling framework serves as the foundation for a more refined treatment of geogrid-stabilized layers in ME design and provides a path toward incorporating observed field benefits into performance-based pavement specifications.

5.2 Finite Element Modeling Framework and Parameter Calibration

To support the translation of field-measured responses into design-relevant parameters, a finite element modeling framework was developed using the C-FLEX flexible pavement analysis tool. Originally created by the U.S. Army Corps of Engineers, C-FLEX enables simulation of nonlinear, stress-dependent behavior of pavement foundation layers and is well suited for evaluating the influence of geosynthetic stabilization on unbound aggregate performance.

The primary goal of the modeling effort was to simulate observed stiffness variations in geogrid-stabilized sections by incorporating depth-specific adjustments to resilient modulus parameters, and to validate the resulting pavement responses against field data from APLT and BE sensors.

5.2.1 Model Configuration and Sublayering Strategy

The finite element mesh was configured to replicate the full-scale pavement test sections constructed as part of the US 20 field project. Each test section consisted of a 12-in.-thick aggregate base layer (INDOT No. 53 aggregate) underlain by a compacted natural sand subgrade. The modeled pavement cross-section reflected field dimensions and layer thicknesses to preserve the fidelity of load transfer mechanisms across interfaces. To capture localized stiffness enhancements associated with geogrid inclusion, the 12-in. base layer was discretized into six sublayers, each 2 in. thick. This approach enabled spatial variation in modulus values within the base and facilitated modeling of the MSL formed in proximity to the geogrid. For the geogrid-stabilized test sections (GG1 and GG2), the

MSL was centered around the known geogrid depth, allowing parameter modifications to be applied to specific sublayers surrounding the geogrid. In all simulations, the geogrid itself was not modeled as an explicit structural element. Rather, its mechanical effect was represented through modulus enhancement factors applied to the sublayers near the geogrid. This approach offers flexibility for modeling geogrid-induced confinement without introducing complex interface behavior or requiring high mesh density around the geogrid.

5.2.2 Material Model

Unbound aggregate materials were modeled using the MEPDG nonlinear stress dependent resilient modulus model:

$$M_R = k_1 p_a \left(\frac{\theta}{p_a}\right)^{k_2} \left(1+\frac{\tau_{oct}}{p_a}\right)^{k_3} \qquad \text{Equation 5.1}$$

where θ is the bulk stress, τ_{oct} is the octahedral shear stress, pa is atmospheric pressure (reference stress), and k_1, k_2, and k_3 are model parameters representing modulus magnitude (or constant term), bulk stress sensitivity, and shear stress sensitivity, respectively. Field-derived deflection measurements from APLT were used to backcalculate the resilient modulus for each section using a forward–inverse approach. The backcalculation procedure employed a layered elastic solution to match measured surface deflections with model outputs. An optimization routine minimized the mean squared error between observed and predicted deflections to yield the baseline k_1, k_2, k_3 values for the control section.

To determine the resilient modulus model parameters k_1, k_2, and k_3 for the aggregate base layer, a multistep backcalculation protocol was developed using field measurements from the APLT loading program and the associated instrumentation. The procedure began with estimating the resilient modulus of the subgrade, M_{Rsg}, for each loading stage using the AASHTO (1993) equation for a homogeneous half-space:

$$M_{R(sg)} = \frac{\left(1-\nu^2\right)P}{\pi r' \delta_{r,r'}} \qquad \text{Equation 5.2}$$

where P is the applied cyclic load, ν is the assumed Poisson's ratio of the subgrade (taken as 0.40), r' is the radial distance three times the loading plate radius, and $\delta_{(r,r')}$ is the measured rebound deflection at that offset. For each stress level, modulus values were averaged over the final five loading cycles to mitigate transient effects and establish representative subgrade behavior.

With the subgrade modulus fixed, the next step involved estimating the resilient deflection at the center of the loading plate using an analytical solution for a two-layer elastic system based on Boussinesq theory. The formulation used is given as follows:

$$\delta_r = \left(1-\nu^2\right)\sigma_0 rf \left[\frac{1}{M_{R(sg)}\sqrt{1+\left(\left(\frac{h}{r}\right)\left(\sqrt[3]{\frac{M_{R(base)}\left(1-\nu_1^2\right)}{M_{R(sg)}\left(1-\nu_2^2\right)}}\right)^2\right)}} + \frac{1-\left(\frac{1}{\sqrt{1+\left(\frac{h}{r}\right)^2}}\right)}{M_{r(base)}} \right] \qquad \text{Equation 5.3}$$

In this equation, ν_1 and ν_2 represent the Poisson's ratios for the base and subgrade, respectively, σ_0 is the applied surface stress, r is the loading plate radius, h is the base layer thickness, and f is a shape factor taken as 8/3 per convention (White et al., 2018). During the calibration, M_{Rsg} was held constant while $M_{R(base)}$ was iteratively adjusted using Microsoft Excel Solver. The Solver routine minimized the mean squared error (MSE) between the measured and calculated rebound deflections, yielding a best-fit modulus value for each APLT stress stage.

Following this deflection matching process, the fitted base moduli were plotted against their corresponding stress states to calibrate the MEPDG resilient modulus model parameters. The bulk stress was computed as the sum of the applied deviator stress and the overburden pressure, using an assumed lateral earth pressure coefficient $K_0 = 0.5$ and the known unit weight of the base material. All stress terms were consistently evaluated at the mid-depth of the aggregate base layer to ensure comparability across sections.

The final backcalculated values of k_1, k_2, and k_3 for each section are presented in Table 5.1. The results show a clear influence of geogrid inclusion on base layer behavior. Compared to the control section, the geogrid-stabilized sections GG1 and GG2 exhibited increased modulus constant term (higher k_1) and reduced stress sensitivities (lower values of k_2 and k_3). These trends confirm that geogrid stabilization enhances the resilient

TABLE 5.1
Estimated MEPDG Model Parameters for Each Test Section.

Section	k_1	k_2	k_3
CS	2611.3	0.61	-0.78
GG1	3312.4	0.37	-0.53
GG2	2897.1	0.29	-0.37

response of the base and reduces its stress dependency under loading.

These parameter sets were subsequently used to derive scalar multipliers, α, -β, and -γ, to quantify the relative enhancements attributed to geogrid stabilization. These multipliers were implemented in the sublayer-based modeling framework to simulate localized stiffness behavior within the MSL, as described in the following section.

5.2.3 Modeling of Geogrid Influence Zone

To account for the localized nature of stiffness enhancement in geogrid-stabilized pavement layers, a sublayer-based modeling approach was developed. This framework discretized the 12-in.-thick unbound aggregate base into six uniform sublayers, each 2 in. thick. The primary goal of this discretization was to simulate the nonuniform modulus distribution induced by geogrid inclusion, especially within the MSL, defined as the 4-in. zone surrounding the geogrid, 2 in. above and 2 in. below the geogrid plane. This formulation allowed the model to reflect spatially varying confinement and interlock effects, which are typically most pronounced near the geogrid and diminish with increasing distance from its location.

The control section, which lacked geogrid stabilization, was used as the baseline for comparison. This section was modeled using a constant set of resilient modulus model parameters across all sublayers: k_1 = 2611.3, k_2 = 0.61, and k_3 = -0.78. In contrast, the geogrid-stabilized sections (GG1 and GG2) were assigned depth-varying model parameters, derived from scaling the control section MEPDG resilient modulus model parameters using adjustment factors α, -β, and -γ. These scaling factors were first computed from the ratio of backcalculated average parameters in GG1 and GG2 relative to the control section. For example, the backcalculated k_1 for GG1 was 3312.4, resulting in an enhancement ratio of approximately 1.27 compared to the control. Recognizing that this ratio represents a layer-averaged effect, a spatial weighting scheme was applied to emphasize the localized stabilization benefit near the geogrid plane. Sublayers intersecting the geogrid were assigned an interaction multiplier of 0.75, adjacent sublayers (2 in. above or below) were given a reduced multiplier of 0.25, and sublayers further away retained the unmodified control section MEDPG resilient modulus model parameters.

The final depth-adjusted model parameters for each sublayer were computed using the following relation:

$$\boldsymbol{k}_{\mathbf{n}} = \left(1 + \left[\delta \times \boldsymbol{interaction}\right]\right) \times \boldsymbol{k}_{\mathbf{n}}^{\boldsymbol{control}}, \quad \boldsymbol{where}\,\delta \in \{\alpha, -\beta, -\gamma\} \qquad \text{Equation 5.4}$$

where the interaction *i* multiplier varies based on the sublayer's proximity to the geogrid, and *i* denotes the sublayer index. Figure 5.1 illustrates the sublayer configuration and interaction zones.

To refine these adjustments, an iterative optimization framework, as shown in Figure 5.2, was developed in Microsoft Excel using Solver. This model was tasked with reproducing the load-dependent composite modulus values derived from the APLT measurements. The seed moduli for the six sublayers were then converted into an overall effective layer modulus ($M_{R,eff}$) using a harmonic mean formulation shown below, which was then fitted against APLT measured base modulus using a harmonic mean formulation:

$$M_{R,eff} = \left(\sum_{i=1}^{n} \frac{h_i}{E_i} \right)^{-1} \qquad \text{Equation 5.5}$$

Here, h_i is the thickness of sublayer *i*, and E_i is its computed resilient modulus value computed using the localized MEPDG parameters. To isolate the impact of modulus variation, bulk and shear stress inputs were held constant across *n* sublayers, using the average values calculated at the mid-depth of the base. This simplification allowed the calibration process to focus on refining the depth profile of stiffness without the added complexity of recalculating internal stress distributions.

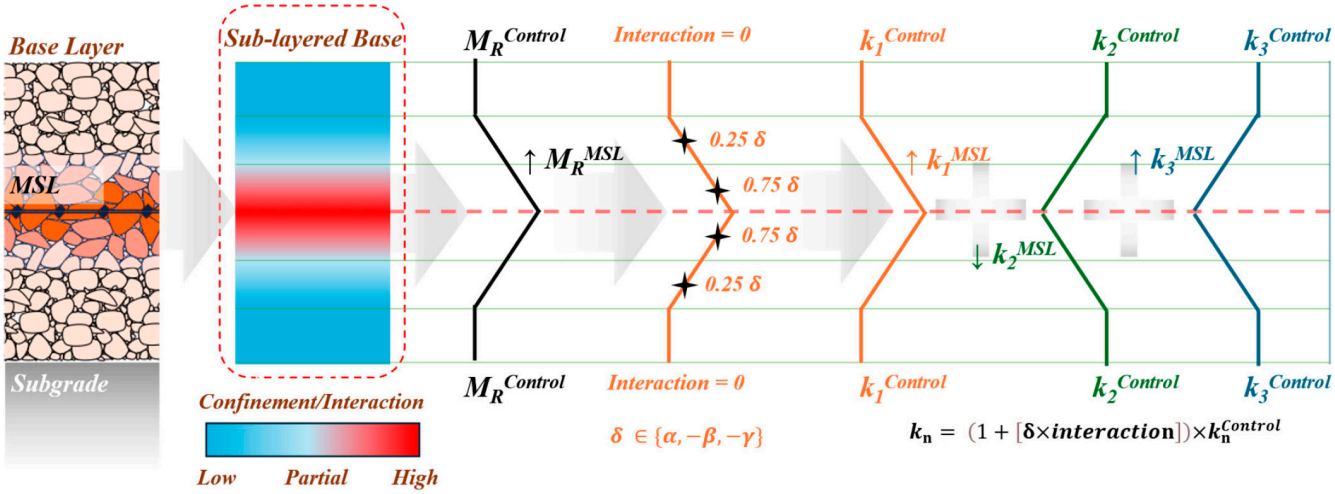

Figure 5.1 Sketch Showing the Division of Aggregate Base Layer Into 2-in. Sublayers With Varying Degrees of Confinement and Associated Changes in MEPDG Model Parameters.

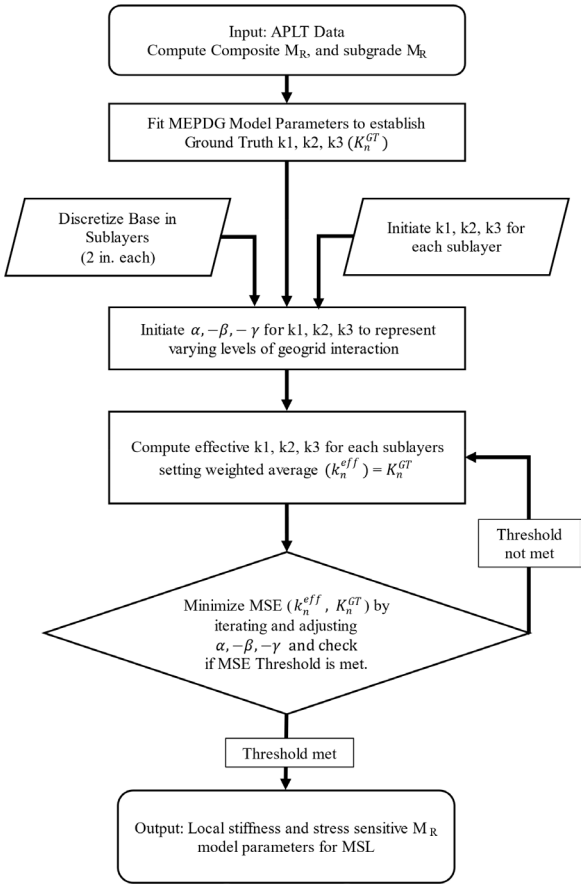

Figure 5.2 Implementation Algorithm for Sublayer Stiffness Assessment.

Solver was used to adjust the scaling factors α, -β, and -γ for each geogrid section. The optimization minimized the MSE between the predicted composite modulus and the APLT-derived modulus at each stress stage. This calibration was performed independently for the GG1 and GG2 sections to ensure accurate representation of the distinct geogrid configurations. The resulting sublayer model parameters were then input into the finite element program C-FLEX to solve for pavement responses and further evaluate the accuracy and practicality of the proposed modeling approach.

By enabling spatially resolved adjustment of resilient modulus model parameters, this sublayer-based modeling framework provides a mechanistic analysis approach and a consistent means of capturing the confinement and interlock effects introduced by geogrid stabilization. It offers a significant improvement over the traditional single-layer or averaged-parameter approaches by more accurately reflecting the true distribution of stiffness enhancements within the stabilized base.

5.2.4 Model Validation and Preparedness for Design Application

Consistent with field testing conditions, a uniform circular load replicating the APLT plate (18-in. diameter) was applied at the surface in the model. The pulsed vertical stress for the plate contact was set at 15 psi (103.4 kPa), corresponding to the conditioning stress state used in the test protocol. This stress state was selected as it had the highest number of repetitions during APLT loading. The subgrade layer was modeled using isotropic nonlinear bilinear material model parameters, extending to a depth sufficient to avoid boundary effects. In C-FLEX, lateral boundaries are constrained horizontally, and the bottom boundary is fixed vertically far away to match negligible deformation at the bottom of the analysis domain.

TABLE 5.2
Model Parameter Adjustment Factors Computed After Backcalculation.

Parameter	No. 53 Aggregate (APLT)	Adjustment Factor for MSL (1 + δ) $where, \delta \in \{\alpha, -\beta, -\gamma\}$	Parameter	MSL
k_1	2611.32	1.44	k_1	3754.3
k_2	0.61	0.17	k_2	0.11
k_3	-0.78	0.17	k_3	-0.13

The C-FLEX pavement model served a dual purpose: (1) validating the hypothesis that geogrid inclusion results in measurable local stiffness enhancements, and (2) producing design-ready resilient modulus inputs reflecting those enhancements. The calibrated modulus distributions were further corroborated against BE sensor-derived shear wave velocity trends, particularly in the MSL region. This modeling framework forms the basis for performance comparison across typical pavement structures and enables estimation of geogrid benefits, which quantify the improvement in critical pavement response due to geogrid stabilization. These concepts are expanded upon in subsequent sections.

The final adjustment factors and corresponding depth-specific MEPDG model parameters used to represent the geogrid influence are summarized in Table 5.2 and Table 5.3, respectively. These values were derived through iterative calibration of sublayer moduli to match the observed composite modulus response from APLT deflection measurements. For the sublayers directly overlapping within the geogrid influence zone, the initial stiffness enhancement backcalculated was the most pronounced, with a modified k_1 value of approximately 3468.6 psi. Adjacent sublayers within the MSL were assigned interpolated parameters based on a piecewise linear distribution, reflecting the diminishing influence of geogrid-induced confinement and interlock away from the geogrid plane, as discussed earlier.

Table 5.2 presents the global adjustment factors, α, β, and γ, applied to the control model parameters for k_1, k_2, and k_3, respectively. These were derived from the ratio of backcalculated values in the stabilized sections to those of the control section. For instance, an adjustment factor of 1.44 was applied to k_1, indicating a 44% increase in modulus constant term in the geogrid-stabilized zone. Meanwhile, both k_2 and k_3 exhibited significant reductions within MSL, suggesting mitigated stress dependency in the presence of geogrid stabilization. These trends are consistent with the confinement mechanism, wherein the geogrid restricts lateral deformation and distributes

TABLE 5.3
Computed Sublayer MEPDG Model Parameters for a Mid-Depth Geogrid Configuration With sample Calculation for k_1

	$k_n = \left(1 + \left[\delta \times interaction\right]\right) \times k_n^{control}$ $where\ \delta \in \{\alpha, -\beta, -\gamma\}$		
Degree of geogrid-induced confinement	k_1	k_2	k_3
No Confinement/Control	2611.32	0.61	-0.78
Partial Confinement	(1 + [0.44 × 0.25]) × 2611.32 = 2897.07	0.19	-0.24
Full Confinement	(1 + [0.44 × 0.75]) × 2611.32 = 3468.57	0.084	-0.11
Full Confinement	(1 + [0.44 × 0.75]) × 2611.32 = 3468.57	0.084	-0.11
Partial Confinement	(1 + [0.44 × 0.25]) × 2611.32 = 2897.07	0.19	-0.24
No Confinement/Control	2611.32	0.61	-0.78

load more uniformly, thus reducing the sensitivity of modulus to bulk and shear stresses.

Table 5.3 illustrates how these adjustment factors were applied to individual sublayers. Using the scaling factor, the parameters were depth-modulated across the base layer. For example, in sublayers intersecting the geogrid (with an interaction factor of 0.75), the enhanced k_1 was calculated as (1+ [0.44×0.75]) × 2611.3 = 3468.6 psi. Adjacent sublayers received lower multipliers of 0.25, modeling enhancement depth-profile in MSL. Sublayers beyond the MSL were assigned the original control parameters, effectively modeling the transition from geogrid-stabilized to non-stabilized aggregate behavior.

This sublayering framework provided the means to simulate localized zone stiffening effects of different geogrid configurations. In the mid-depth geogrid section (GG2), the enhancements were concentrated around the center of the base, while in the interface geogrid section (GG1), the modifications were applied near the bottom sublayers. This differentiation aligns with expected geogrid-induced confinement zones and confirms that the magnitude and location of stiffness enhancement depend on geogrid placement depth. The resulting parameter distributions enable a realistic and mechanistically grounded representation of pavement foundation behavior.

Compared to conventional approaches that apply a uniform modulus across the entire base layer, this method allows for refined modeling of localized geogrid effects, enabling closer alignment with in-situ measured responses. It also improves compatibility with finite element simulations and mechanistic design frameworks. The calibrated MEPDG model parameters from this process were subsequently incorporated into the finite element program C-FLEX to solve for pavement responses and compare them with APLT-measured deflection and modulus trends. These efforts supported the validation of the sublayer-based modeling approach and demonstrated its applicability for representing the complex, depth-dependent stiffness behavior of geogrid-stabilized base layers.

5.3 Validation and Applicability to Typical Pavement Layer Configurations

To evaluate the accuracy and practical utility of the sublayer-based modeling framework, predicted deflection basins generated using calibrated MEPDG parameters were compared against field-measured deflections obtained from the APLT loading program. The C-FLEX finite element platform was used to simulate the three test sections, control (CS), geogrid at the interface (GG1), and geogrid at mid-depth (GG2), under identical loading conditions. The applied surface stress was 15 psi (103.4 kPa), consistent with the plate contact stress used during APLT conditioning for matching purposes.

As shown in Figure 5.3, the predicted deflection basins closely matched the measured rebound deflections for all sections, confirming the model's ability to accurately capture both the magnitude and shape of the surface deflection profiles. Among the three configurations, the control section, shown in Figure 5.3a, exhibited the deepest and broadest deflection basin, consistent with a lower composite stiffness. In contrast, Figure 5.3b and Figure 5.3c illustrate the narrower and shallower deflection basins associated with GG1 and GG2, respectively. These patterns confirm that the calibrated sublayer MEPDG model parameters effectively reflect the increased stiffness induced by geogrid inclusion. The strong agreement between the measured results and model predictions validates the sublayer model parameter adjustment strategy and supports the physical relevance of the modified k_1, k_2, and k_3 values.

To further examine the influence of geogrid stabilization on critical pavement responses, the validated model was used to predict vertical deviator strain and stress on top of subgrade under the application of surface stresses ranging from 10 psi up to 40 psi. These responses are fundamental to rutting predictions and are central to ME pavement design methodologies. The vertical compressive strains predicted on top of the subgrade are summarized in Figure 5.4. The geogrid-stabilized sections exhibited consistently lower strain levels than the control section across all applied stress levels. For example, at an applied stress of 10 psi (69 kPa), the control section exhibited a vertical strain of 189 micro strain (με), while GG1 and GG2 exhibited strains of 146 με and 150 με, respectively. These correspond to reductions of approximately 23% for GG1 and 21 percent for GG2. This trend of strain attenuation, though slightly less pronounced at higher stress levels, remained consistent across the loading spectrum and underscores the role of geogrid in enhancing confinement and mitigating load-induced deformation.

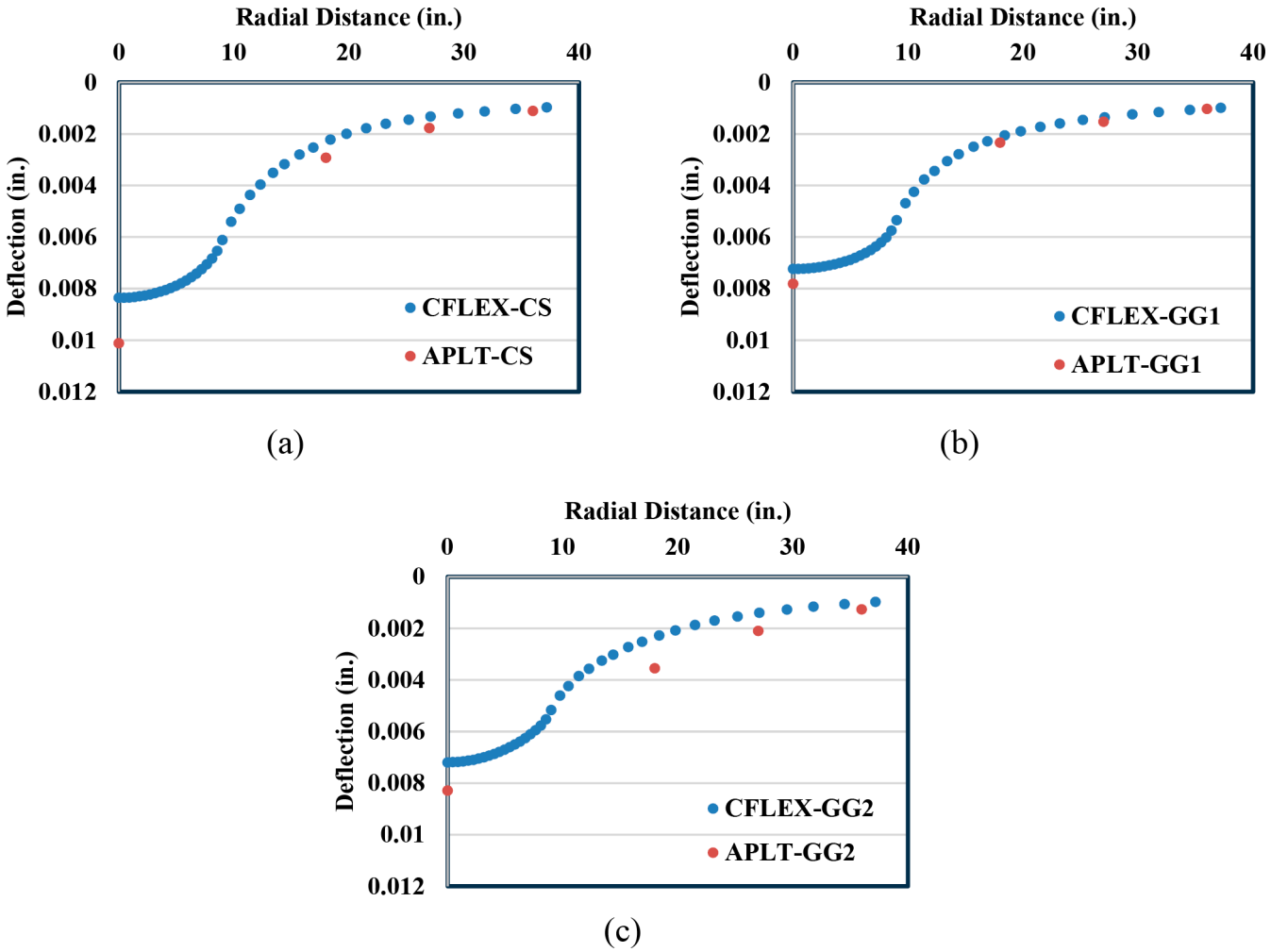

Figure 5.3 Validation Matching of C-FLEX FE Analysis Predicted Deflection Basins (15-psi Surface Stress Loading and Computed Sublayer-Based Modeling Inputs) With APLT Measured Deflection Pools for (a) CS, (b) GG1, and (c) GG2 (1 in. = 25.4 mm; 1 psi = 6.9 kPa).

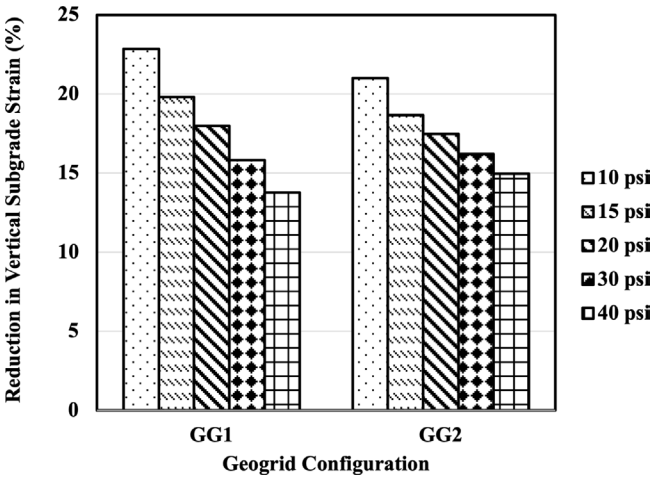

Figure 5.4 Estimated Vertical Strain Reduction on Top of Subgrade With Legend Showing APLT Pulsed Stress Applied on Top of Aggregate Layer (1 psi = 6.9 kPa).

Vertical stress responses predicted on top of subgrade followed a complementary trend. As shown in Figure 5.5, both GG1 and GG2 exhibited lower transmitted stresses compared to the control section. At a 30-psi (207 kPa) loading condition, the vertical subgrade stress measured in the control section was approximately 13.9 psi, while GG1 and GG2 recorded values of 12.5 psi and 12.3 psi, respectively. These values reflect reductions of 9.5% and 11.2% relative to the control and highlight the improved load distribution and stress dispersion facilitated by the geogrid-stabilized aggregate base layers. The slightly superior performance of GG2 in reducing vertical stress suggests a more effective bridging mechanism across the aggregate layer thickness when the geogrid is placed at mid-depth.

As an observation, the strain and stress response results emphasize two distinct but complementary benefits of geogrid stabilization: a significant reduction in vertical deformation and a notable attenuation of transmitted stress to the subgrade. The enhanced strain reduction observed in GG1 indicates stronger confinement

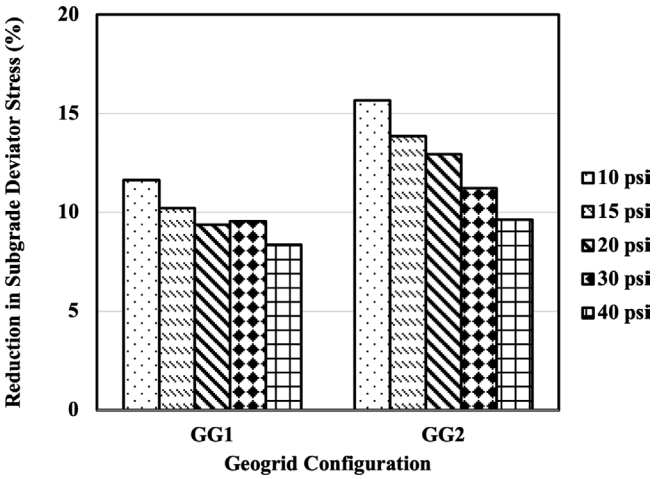

Figure 5.5 Estimated Top of Subgrade Vertical Stress Reduction With Legend Showing APLT Pulsed Stress Applied on Top of Aggregate Layer (1 psi = 6.9 kPa).

near the base–subgrade interface, while the lower stresses observed in GG2 suggest a broader lateral load distribution across the aggregate matrix. These mechanistic analysis insights emphasize the importance of evaluating multiple response metrics when assessing the effectiveness of stabilization strategies and determining optimal geogrid placement configurations.

To corroborate these findings, field measurements from embedded BE Field sensors were also examined. These sensors captured Vs at the same locations and following each APLT load stage, thereby providing high-resolution, independent validation of local stiffness characteristics. This paired testing approach enabled a direct comparison between BE-derived stiffness trends and those inferred from APLT-based modulus backcalculation and C-FLEX simulations. At a high stress level of 38 psi (262.2 kPa), enhancement ratios (ER_{BE}) of approximately 1.07 were recorded in both GG1 and GG2 relative to the control, indicating a 7% increase in shear wave velocity. Since stiffness is proportional to the square of shear wave velocity, this corresponds to an approximate 14% increase in local stiffness. At the lower stress level of 13 psi (89.7 kPa), ER_{BE} values were approximately 1.11, translating to a 23% increase in stiffness. These BE-derived enhancement values are in strong agreement with the strain and stress reductions observed in the finite element modeling predictions. Specifically, the 23% and 21% reductions in vertical strain and the 9.5% and 11.2% reductions in vertical stress observed for GG1 and GG2, respectively, mirror the BE-measured stiffness improvements. This consistency confirms the robustness of the calibrated MEPDG model parameters and underscores the value of integrating multiple sensing and modeling approaches to fully capture the mechanistic effects of geogrid stabilization.

5.4 Evaluation of Typical Indiana Pavement Sections

To evaluate the applicability of the sublayer modeling framework and geogrid influence across realistic pavement configurations, a parametric study was conducted using the calibrated MEPDG model parameters. The study considered typical INDOT pavement designs for low-volume, medium-volume, high-volume, and interstate classifications, as illustrated in Figure 5.6. These pavement sections varied primarily in terms

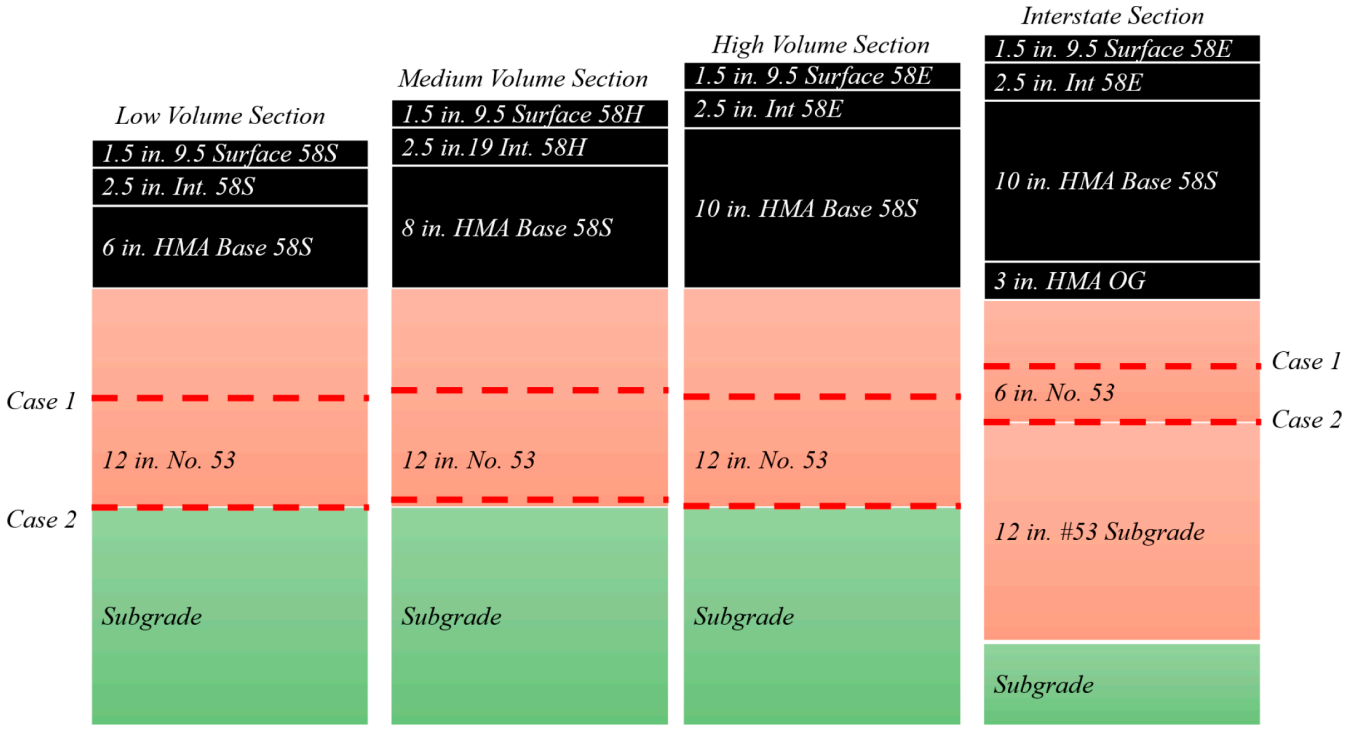

Figure 5.6 Typical INDOT Pavement Sections Analyzed for the Parametric Study.

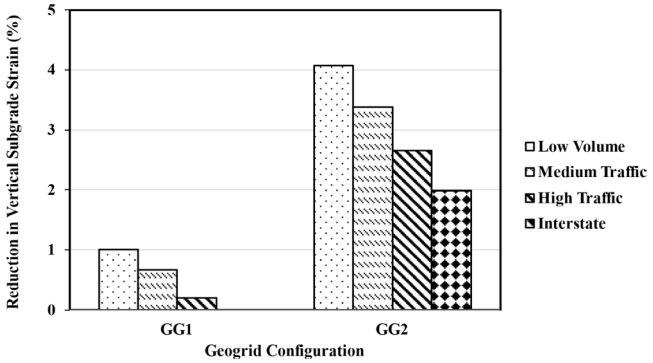

Figure 5.7 Estimated Vertical Strain Reduction on Top of Subgrade for Typical INDOT Pavement Sections With Legend Showing APLT Pulsed Stress Applied on Top of Aggregate Layer.

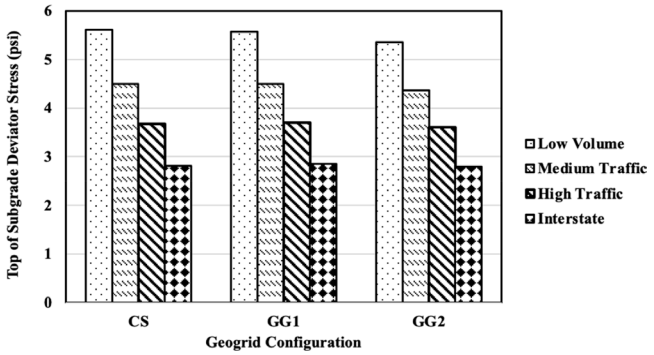

Figure 5.8 Estimated Top of Subgrade Vertical Stress Reduction With Legend Showing APLT Pulsed Stress on Top of Aggregate Layer for the Typical INDOT Pavement Sections (1 psi = 6.9 kPa).

of HMA thickness and base layer design. Per INDOT (2013) Part 6, Chapter 601, Figure 601-5C, the combined HMA layer thicknesses were modeled as 10 in. in the low-volume section, 12 in. for the medium-volume section, 14 in. for the high traffic section, and 17 in. in the interstate section. The base layer thickness remained consistent at 12 in. in the first three sections and increased to 18 in. in the interstate design.

Like the previous investigations in this project, three modeling configurations were evaluated for each pavement type: (1) a CS without geogrid, (2) GG1 with geogrid placed at the base–subgrade interface, and (3) GG2 with geogrid positioned at mid-depth of the base layer. The calibrated sublayer MEPDG model parameters from earlier analyses were used as inputs. C-FLEX was used to predict mechanistic responses under a representative equivalent single axial load (ESAL) of 18 kips with a target stress of 80 psi distributed over 6 in. of tire contact.

Figure 5.7 shows the estimated percentage reduction in vertical compressive strain on top of the subgrade. GG2 consistently outperformed GG1 in reducing strain across all traffic classes. In the low-volume section, GG2 yielded the highest strain reduction, exceeding 4%. This value decreased progressively with traffic class, falling to below 2% for the interstate configuration. In contrast, GG1 produced minimal strain reduction across the board, with values below 1% for most designs. These findings suggest that mid-depth placement (GG2) is more effective in mitigating vertical deformation, particularly in sections with thinner asphalt layers.

Figure 5.8 illustrates the top-of-subgrade vertical stress responses for the three configurations. For the stabilized systems, there was notably a marginal improvement over the control section. The reduced effectiveness of geogrid in thicker pavement systems may be attributed to the confining effect of the HMA layer. In thicker HMA sections, stress attenuation is largely governed by the asphalt layers themselves, which limits the influence of MSL. Yet, mid-depth placement allows the geogrid to directly engage with the most actively stressed portion of the aggregate base, enhancing lateral load distribution and confining response.

It is also important to recognize that while the predicted improvements in stress and strain are more evident in the low-volume configurations, the benefits of geogrid stabilization are not limited to short-term deflection behavior. Over time, aggregates in control sections tend to experience stiffness degradation due to particle reorientation and displacements resulting in deformation accumulation. Geogrid-stabilized sections, however, retain modulus more effectively due to the confinement and mechanical interlock provided by the geogrid. These long-term performance benefits are not fully captured in finite element method simulations, such as those performed in C-FLEX, yet they are critical for accurate pavement performance prediction.

Therefore, even when the short-term differences between control and stabilized sections appear modest in thicker pavement designs, practitioners should interpret these results with the understanding that geogrid-stabilized bases are likely to provide better modulus retention and structural stability over time. This distinction is particularly relevant for ME design approaches, where accurate representation of long-term layer properties is essential for life-cycle performance prediction and for accurately predicting pavement rutting performance benefits associated with the traffic benefit ratio.

5.5 Summary

ME pavement design relies on accurate characterization of pavement foundation materials, particularly the resilient modulus of unbound aggregate base layers. However, current design procedures often treat geogrid-stabilized and nonstabilized bases as equivalent, typically assigning a fixed modulus value regardless of geogrid. This approach overlooks the mechanical benefits introduced by geogrid inclusion, including improved stiffness, enhanced confinement, and redistribution of stress. To address this limitation, the modeling framework presented in this chapter demonstrates a systematic approach to quantifying and integrating the effects of geogrid stabilization into design procedures.

Field testing conducted along the US 20 test site included APLT, BE shear wave velocity measurements, and embedded pressure cell data. These techniques revealed consistent trends of increased local and composite stiffness in geogrid-stabilized sections compared to the control. Building on these findings, a

sublayer-based finite element modeling framework was developed using the C-FLEX analysis tool. The model incorporated depth-dependent adjustments to the resilient modulus, represented through the MEPDG resilient modulus model k_1, k_2, and k_3 parameters, and applied scalar multipliers to simulate the MSL surrounding the geogrid.

The modeling effort involved backcalculation of stress-dependent modulus values from field data, calibration of model parameters, and validation against measured surface deflections and BE-derived stiffness profiles. Results showed that geogrid placement at mid-depth (GG2) yielded the highest improvements in both strain attenuation and stress dispersion, while the geogrid placed at the base–subgrade interface (GG1) also provided measurable benefits. Compared to the control section, GG2 demonstrated a 23% reduction in vertical strain and an 11% reduction in subgrade stress, aligning with a 14 to 23% increase in BE-derived local stiffness. These consistent findings from independent methods confirm the robustness of the modeling framework and the effectiveness of geogrid stabilization.

A subsequent parametric study applied a calibrated modulus modeling framework to a range of typical INDOT pavement designs varying in traffic classification and HMA thickness. The results revealed that the relative benefits of geogrid stabilization were more pronounced in thinner pavements, such as low-volume roads, where geogrids directly influenced stress and strain distributions within the aggregate base. While thicker HMA layers in higher-volume pavements reduced the short-term influence of the geogrid on subgrade responses, the long-term modulus retention benefits remain quite relevant. In control sections, aggregate modulus tends to degrade over time due to cumulative deformation and loss of interlock. In contrast, geogrid-stabilized sections preserve structural integrity more effectively due to confinement mechanisms, a benefit not fully captured in short-duration simulations but critical for long-term performance.

Overall, the developed modeling framework offers a mechanistically consistent, field-validated approach to incorporating geogrid stabilization effects into ME pavement design. It provides a clear pathway for translating sensor-derived stiffness trends and load response measurements into design-relevant parameters that can improve the accuracy of performance predictions. These outcomes support the adoption of refined resilient modulus inputs and benefit ratios for stabilized bases in INDOT's pavement design procedures.

6. CONCLUSIONS AND RECOMMENDATIONS

6.1 Overview of Key Research Outcomes

This research, conducted along a reconstructed segment of US 20 in Elkhart County, Indiana, aimed to provide INDOT with a mechanistic analysis and design framework for geogrid-stabilized pavement aggregate base layers. By integrating embedded instrumentation, nondestructive field testing, and mechanistic analysis through advanced numerical modeling, the study provided a comprehensive evaluation of the structural benefits associated with geogrid stabilization immediately after construction, and over extended traffic and environmental loading. The data informed base course sublayering approach adopted in the research supports development of an improved resilient modulus characterization. The approach was implemented in evaluating typical INDOT pavement sections and the observations further support the inclusion of geogrid-specific enhancements in performance-based specifications.

Three instrumented test sections were constructed, including a control section with no geogrid-stabilization and two sections with geogrids placed at two depths within the base layer: (i) at base–subgrade interface and (ii) at mid-depth of the base layer. Data from innovative BE Field sensors, EPCs, and APLT were contextualized together to quantify the mechanical responses of the stabilized and no-geogrid control sections across a range of conditions. The results confirmed that geogrid-stabilization leads to measurable increases in local stiffness and improved stress distribution characteristics. Notably, data from the field experiment linked geogrids with enhanced stiffness retention and lower stress transmission to the subgrade, particularly under repeated traffic loading and during seasonal transitions.

Paired APLT–BE measurements provided valuable insights into the interaction between multilayer and local stiffness behaviors. The BE enhancement ratio (ER_{BE}), derived from shear wave velocity (Vs) measurements under staged APLT loading, confirmed a localized stiffening effect in the vicinity of the geogrid. The Vs enhancement ranged from 7% to 11 % with higher benefits observed under realistic field-stress conditions. This implied a much greater increase in the localized stress-dependent modulus behavior, which highlighted the inadequacy of treating geogrid-stabilized and no-geogrid bases as equivalent in terms of modulus characterization, as is often done in current INDOT design specifications.

The extended monitoring program further demonstrated that geogrid-stabilized sections maintained higher as-built base layer stiffnesses and exhibited lower subgrade vertical strain and stress levels throughout seasonal cycles and post-construction traffic operation. Particularly, BE sensors revealed that the control section experienced a steady reduction in shear wave velocity, an indicator of layer stiffness. These observations confirm and quantify the formation of a durable MSL in stabilized sections which remained intact through seasonal changes with retained high stiffnesses in geogrid influence zones, which play a critical role in preserving pavement performance under environmental and traffic-induced stresses.

To operationalize these findings in pavement design, a sublayer-based aggregate material modulus model parametrization framework was developed and implemented using the C-FLEX program. The model incorporated stress-dependent resilient modulus behavior through the MEPDG formulation and enabled the assignment of distinct modulus properties to 2-in.-thick sublayers within the base. Scalar multipliers were used to calibrate the effects of geogrid inclusion on modulus parameters (k_1, k_2, k_3), allowing simulation of the stiffness improvement and stress sensitivities of the MSL generating pavement responses which were validated against field measurements. The model demonstrated strong agreement with observed APLT deflection basins

and provided a robust platform for mechanistic performance comparisons across the different geogrid-stabilized design configurations.

Finally, a finite element modeling study applied the validated geogrid-stabilized base model to typical INDOT pavement structures, revealing that geogrid stabilization can measurably improve critical pavement responses. Though this benefit is dependent on the overall pavement structure with stiffness of HMA governing the stress transmission to subgrade over the MSL, the retention of modulus on geogrid stabilized sections, as confirmed with BE Field measurements during extended study period, offers a pathway to maintain constructed performance while non-stabilized sections experience a reduction in performance metrics and increasing the risk of distress development. These outcomes not only confirm the technical value of geogrid stabilization but also offer implementable design framework, such as with the sublayer MEPDG resilient modulus model parameter inputs developed for the base layer, for implementation in ME pavement design frameworks.

6.2 Recommendations for INDOT Pavement Design Practice

The findings from this study offer actionable insights to improve the design, evaluation, and specification of geogrid-stabilized pavement foundations in Indiana. Based on field observations, long-term monitoring data, and validated finite element modeling, the following recommendations are provided to support the integration of geogrid benefits into INDOT's mechanistic–empirical design practices.

6.2.1 Differentiate Resilient Modulus Inputs for Geogrid-Stabilized and Non-Stabilized Bases

Current INDOT design procedures assign a fixed resilient modulus of 15 ksi (103.5 MPa) to all aggregate base layers, regardless of geogrid inclusion. This simplification does not reflect the enhanced mechanical behavior observed in this study. It is recommended that geogrid-stabilized bases be assigned resilient modulus inputs adjusted according to geogrid location in the layer configuration, either through direct parameter modification (k_1, k_2, k_3) or through the application of scalar enhancement factors derived from backcalculated and validated field data.

To further support implementation, Table 6.1 presents sublayer-based resilient modulus values (in ksi) for geogrid implementation schemes similar to GG1 (base–subgrade interface) and GG2 (mid-depth of base) under varying deviator stress levels, as obtained from calibrated finite element simulations validated against field measurements. These values reflect stress-dependent stiffness behavior within the geogrid influence zone and can help improve current INDOT Pavement ME design inputs. It is encouraged that INDOT engineers carefully select these values based on structural resemblance with the one presented in this study.

The above resilient modulus suggestions were based on the biaxial geogrid with a 33 mm square aperture paired with No. 53 aggregate materials in this study. Any other combinations of geogrid types and aggregate materials should be carefully studied prior to implementation of any enhanced modulus values. Recent studies supported by other transportation agencies can further guide these decisions. One such study by Wang et al. (2025) presents data on various geogrid and aggregate material combinations. It is also anticipated that once the AASHTOWare Pavement ME software functionality is developed to incorporate stress-dependent resilient modulus model parameters, the results presented in Chapter 5 of this report will be readily available to INDOT to utilize the enhanced k_1, k_2, and k_3 values for each of the two implementations, that is, at bottom and mid-depth of geogrid stabilization in aggregate layers.

TABLE 6.1
Recommeded Resilient Modulus Values (ksi) for GG1 and GG2 Implementation for Various Deviator Stress Levels.

Deviator Stress (psi)	GG1 (interface)	GG2 (mid-depth)
5	22.9	23.6
10	19.7	20.5
15	18.2	19.0
20	17.3	18.1
30	16.4	17.2
40	15.9	16.7

6.2.2 Incorporate Sublayer-Specific Modulus Assignments for MSLs

The stress-dependent improvements observed near the geogrid location were localized and depth-specific. The use of a sublayer-based modeling approach allowed these enhancements to be accurately represented. INDOT is encouraged to implement a similar sublayer-based approach when characterizing geogrid-stabilized bases. This would allow more accurate representation of base course stiffness gradients and improve vertical strain and stress predictions on top of subgrade. Notably, a calibrated parameterization framework for the MEPDG aggregate resilient modulus model parameters revealed a 44% increase in initial stiffness constant term (k_1) and reduced bulk and shear stress sensitivities (lower k_2, k_3) by up to 83% within the MSL surrounding the geogrid.

6.2.3 Prioritize Geogrid Placement for Enhanced Stiffness Retention

Long-term BE sensor data and pressure cell measurements indicated that geogrid placement at mid-depth was particularly effective in enhancing base layer stiffness and minimizing stress transmission to the subgrade. However, for typical INDOT base layer thicknesses, placing geogrids at or near subgrade is recommended to achieve a balance between construction feasibility and modulus maintenance. On the other hand, placing geogrids at mid-depth can help alleviate pavement distress development especially when pavements are built on soft natural subgrades.

6.2.4 Validate Stabilization Benefits with Field-Deployable Nondestructive Testing

Paired APLT–BE measurements proved useful in distinguishing stiffness characteristics between geogrid-stabilized and

nonstabilized aggregate layers. INDOT may consider incorporating this paired testing approach into project-level quality assurance or research evaluations. These tools enable rapid, nondestructive characterization of modulus profiles and can help verify the formation and effectiveness of the MSL during construction.

6.2.5 Support Calibration of Mechanistic Models with Embedded Sensor Data

The study demonstrated that long-term embedded sensors (e.g., BE field sensors and pressure cells) provide valuable data for validating pavement performance and supporting model calibration. INDOT may consider expanding the use of such instrumentation in test sections or pilot projects to improve the empirical foundation for design recommendations and further reduce uncertainty in resilient modulus characterization.

Together, these recommendations aim to bridge the gap between research findings and practical implementation. By accounting for the stiffness enhancements and long-term performance benefits associated with geogrid stabilization, INDOT can advance toward more accurate, durable, and cost-effective pavement foundation design practices.

6.3 Suggestions for Future Research

While this study offers a comprehensive evaluation of geogrid-stabilized pavement foundations under in-situ and laboratory conditions, several areas of future research are identified to further advance the understanding, application, and optimization of geosynthetic stabilization in pavement systems.

6.3.1 Expansion of In-Situ Monitoring across Diverse Soil and Climatic Conditions

The current study was conducted on a sandy subgrade in Northern Indiana, where seasonal freeze-thaw cycles and moderate moisture variability were present. To enhance generalizability, future research should include test sections across a range of subgrade types (e.g., clayey, silty) and climatic regions. This would allow for assessment of how subgrade plasticity, moisture retention, and frost susceptibility influence the performance of geogrid-stabilized layers.

6.3.2 Evaluation of Different Geogrid Types and Properties

Only one geogrid type and aperture geometry were evaluated in this study. Comparative testing across a broader selection of commercially available geogrids, including variations in aperture size, junction stiffness, and aperture shape, would help establish more robust correlations between material design input properties and observed performance outcomes. This, in turn, could also better inform material selection guidelines for DOT engineers.

6.3.3 Integration of MSL Representation into Pavement ME Software

The finite element sublayer modeling approach developed in this study offers a path toward incorporating MSL behavior into AASHTOWare Pavement ME or similar ME design platforms. Future work should aim to incorporate the ability to model more than six layers in Pavement ME software for accurate Level 1 modeling of pavement aggregate bases and subbases.

By pursuing these future research directions, transportation agencies and researchers can continue to improve the design, specification, and monitoring of geogrid-stabilized pavement foundations, leading to more resilient and cost-effective infrastructure across varied service environments.

REFERENCES

American Association of State Highway and Transportation Officials. (1993). *AASHTO guide for design of pavement structures.*

American Association of State Highway and Transportation Officials. (1999). *Standard method of test for determining the resilient modulus of soils and aggregate materials* (AASHTO T 307-99).

Al-Qadi, I. L., Dessouky, S. H., Kwon, J., & Tutumluer, E. (2012). Geogrid-reinforced low-volume flexible pavements: Pavement response and geogrid optimal location. *Journal of Transportation Engineering*, *138*(9), 1083–1090. https://doi.org/10.1061/(ASCE)TE.1943-5436.0000409

Al-Qadi, I. L., Tutumluer, E., & Dessouky, S. (2006). Construction and instrumentation of-full-scale geogrid reinforced flexible pavement test sections. In I. L. Al-Qadi (Ed.), *Airfields and highway pavements* (pp. 131–142). American Society of Civil Engineers. https://doi.org/10.1061/40838(191)12

Byun, Y.-H., Qamhia, I. I. A., Kang, M., Tutumluer, E., & Wayne, M. H. (2023). Modeling geogrid-stabilized aggregate base courses considering local stiffness enhancement. *Geosynthetics International*, *31*(6), 888–897. https://doi.org/10.1680/JGEIN.23.00086

Byun, Y.-H., & Tutumluer, E. (2017). Bender elements successfully quantified stiffness enhancement provided by geogrid–aggregate interlock. *Transportation Research Record*, *2656*(1), 31–39. https://doi.org/10.3141/2656-04

Byun, Y.-H., Tutumluer, E., Feng, B., Kim, J. H., & Wayne, M. H. (2019). Horizontal stiffness evaluation of geogrid-stabilized aggregate using shear wave transducers. *Geotextiles and Geomembranes*, *47*(2), 177–186. https://doi.org/10.1016/J.GEOTEXMEM.2018.12.015

Giroud, J. P. (2009). An assessment of the use of geogrids in unpaved roads and unpaved areas. In *Proceedings of the jubilee symposium on polymer geogrid reinforcement* (pp. 23–36), Institution of Civil Engineers.

Hicks, R. G., & Monismith, C. L. (1971). Factors influencing the resilient response of granular materials. *Highway Research Records*, 345, 15–31.

Husain, S. F., Abbas, M. S., Wang, H., Qamhia, I. I. A., Tutumluer, E., Wallace, J., & Hammond, M. (2024). A laboratory-scale evaluation of smart pebble sensors embedded in geomaterials. *Sensors*, *24*(9), 2733. https://doi.org/10.3390/s24092733

Husain, S. F., Tutumluer, E., Qamhia, I. I. A., & Becker, P. (2025). Quantifying geogrid benefits in highway pavements with in-situ testing and bender element field sensors. In H. Ozer & Q. Watkins (Eds.), *Airfield and highway pavements 2025* (pp. 1–9). American Society of Civil Engineers. https://doi.org/10.1061/9780784486214.001

Indiana Department of Transportation. (2013). *Indiana design manual*: *Part 6, Chapter 601*. https://www.in.gov/dot/div/contracts/design/Part%206/Chapter%20601%20-%20Pavement%20Design%20Process.pdf

Kang, M. (2023). *Development and application of bender element field sensor for pavement base/subbase modulus characterization and*

geogrid effectiveness evaluation [Doctoral dissertation, University of Illinois Urbana-Champaign]. IDEALS. https://hdl.handle.net/2142/122136

Kang, M., Qamhia, I. I. A., Tutumluer, E., Hong, W. T., & Tingle, J. S. (2021). Bender element field sensor for the measurement of pavement base and subbase stiffness characteristics. *Transportation Research Record*, *2675*(8), 394–407. https://doi.org/10.1177/0361198121998350

Kwon, J., & Tutumluer, E. (2009). Geogrid base reinforcement with aggregate interlock and modeling of associated stiffness enhancement in mechanistic pavement analysis. *Transportation Research Record*, *2116*(1), 85–95. https://doi.org/10.3141/2116-12

Kwon, J., Tutumluer, E., & Al-Qadi, I. L. (2009). Validated mechanistic model for geogrid base reinforced flexible pavements. *Journal of Transportation Engineering*, *135*(12), 915–926. https://doi.org/10.1061/(ASCE)TE.1943-5436.0000046

Lee, H. S. (2017). *Recommended practice for incorporating geogrids in ME pavement design*. https://www.researchgate.net/publication/328571299

Lee, J.-S., & Santamarina, J. C. (2005). Bender elements: Performance and signal interpretation. *Journal of Geotechnical and Geoenvironmental Engineering*, *131*(9), 1063–1070. https://doi.org/10.1061/(ASCE)1090-0241(2005)131:9(1063)

Leonardi, G., Lo Bosco, D., Palamara, R., & Suraci, F. (2020). Finite element analysis of geogrid-stabilized unpaved roads. *Sustainability*, *12*(5). https://doi.org/10.3390/su12051929

Liu, S., Huang, H., Qiu, T., & Kwon, J. (2016). Effect of geogrid on railroad ballast particle movement. *Transportation Geotechnics*, *9*, 110–122. https://doi.org/10.1016/j.trgeo.2016.08.003

Luo, J., Huang, H., Qamhia, I. I. A., Tutumluer, E., & Tingle, J. S. (2021). C-FLEX advanced finite element analysis program for flexible pavement analysis and design. *Transportation Research Record*, *2675*(9), 1238–1249. https://doi.org/10.1177/03611981211006724

Nazzal, M. D. (2007). *Laboratory characterization and numerical modeling of geogrid reinforced bases in flexible pavements* [Doctoral dissertation, Louisiana State University]. LSU Doctoral Dissertations. 3889. https://doi.org/10.31390/gradschool_dissertations.3889

Qamhia, I., & Tutumluer, E. (2021). *Evaluation of geosynthetics use in pavement foundation layers and their effects on design methods* (Illinois Center for Transportation Report No. FHWA-ICT-21-020). University of Illinois at Urbana-Champaign. https://doi.org/10.36501/0197-9191/21-025

Santamarina, J. C., Klein, A., & Fam, M. A. (2001). Soils and waves: Particulate materials behavior, characterization and process monitoring. *Journal of Soils and Sediments*, *1*, 130. https://doi.org/10.1007/BF02987719

Seed, H. B., Mitry, F. G., Monismith, C. L., & Chan, C. K. (1967). Factors influencing the resilient deformations of untreated aggregate base in two-layer pavements subjected to repeated loading. *Highway Research Record*, *190*, 19–57.

Seyhan, U., & Tutumluer, E. (2002). Anisotropic modular ratios as unbound aggregate performance indicators. *Journal of Materials in Civil Engineering*, *14*(5), 409–416. https://doi.org/10.1061/(asce)0899-1561(2002)14:5(409)

Suku, L., Prabhu, S. S., & Sivakumar Babu, G. L. (2017). Effect of geogrid-reinforcement in granular bases under repeated loading. *Geotextiles and Geomembranes*, *45*(4), 377–389. https://doi.org/10.1016/J.GEOTEXMEM.2017.04.008

Tutumluer, E. (2008). State of the art: Anisotropic characterization of unbound aggregate layers in flexible pavements. In Z. You, A. R. Abbas, & L. Wang (Eds.), *Pavements and materials: Modeling, testing, and performance* (pp. 1–16). American Society of Civil Engineers. https://doi.org/10.1061/41008(334)1

Tutumluer, E., & Seyhan, U. (1999). Laboratory determination of anisotropic aggregate resilient moduli using an innovative test device. *Transportation Research Record*, *1687*(1), 13–22. https://doi.org/10.3141/1687-02

Wang, H., Kang, M., Qamhia, I. I. A., Tutumluer, E., Wayne, M. H., & Shoup, H. (2023). Evaluation of open-graded aggregates stabilized with a multi-axial geogrid using a large-scale triaxial test set-up. *Transportation Research Record*, *2611*(10). https://doi.org/10.1177/03611981231161351

Wang, H., Qamhia, I. I. A., Tutumluer, E., & Kim, Y. (2025). *Effectiveness of geosynthetics in soil/aggregate stabilization—Evaluation Using bender element sensor technology* (Illinois Center for Transportation Report No. FHWA-ICT-25-007). University of Illinois Urbana-Champaign. https://doi.org/10.36501/0197-9191/25-007

Wayne, M., Boudreau, R., & Kwon, J. (2011). Characterization of mechanically stabilized layer by resilient modulus and permanent deformation testing. *Transportation Research Record*, *2204*(1), 76–82. https://doi.org/10.3141/2204-10

White, D. J., & Vennapusa, P. K. R. (2017). In situ resilient modulus for geogrid-stabilized aggregate layer: A case study using automated plate load testing. *Transportation Geotechnics*, *11*, 120–132. https://doi.org/10.1016/j.trgeo.2017.06.001

White, D. J., Vennapusa, P., Tutumluer, E., Vavrik, W., Moaveni, M., & Gillen, S. (2018). Spatial verification of modulus for pavement foundation system. *Transportation Research Record*, *2672*(52), 333–346. https://doi.org/10.1177/0361198118782266

Zornberg, J. G. (2012). *Geosynthetic-reinforced pavement systems* [Keynote pager]. Fifth European Geosynthetics Conference (EuroGeo5), Valencia, Spain. https://sites.utexas.edu/zornberg/files/2022/03/Zornberg_2012e.pdf

APPENDICES

Appendix A. Step-by-Step Procedure for Sublayer-Based Analysis Framework for Geogrid-Stabilized Bases

Appendix-A. Step-by-Step Procedure for Sublayer-Based Analysis Framework for Geogrid-Stabilized Bases

Step 1: Conduct Laboratory or Field Data Collection

a) Determine the geogrid aggregate combination for generation of design inputs.

I. IF biaxial (33 mm aperture) and No. 53 aggregate gradation, select this report recommendation.
II. ELSE perform in-situ/laboratory testing similar to this report.

Step 2: Configure Pavement Geometry and Discretize the Base Layer

a) Initiate the base layer. Typical 12 in. INDOT No. 53 aggregate over subgrade.
b) Discretize the base into sublayers, typical to discretize 12 in. layer in six 2 in. thick sublayers.
c) Assign geogrid location as either at the interface (GG1) or mid-depth (GG2) as designed.

Step 3: Estimate Initial Moduli Using APLT Deflections

a) Compute subgrade modulus M_R using AASHTO (1993) homogeneous half-space solution from repeated loading data.
b) Fix subgrade modulus and use a two-layer elastic theory to backcalculate base modulus at each stress stage.
c) Use Excel Solver to minimize the error between measured and predicted rebound deflections.

Step 4: Fit Stress-Dependent Resilient Modulus Parameters

a) Use MEPDG model:

$$M_R = k_1 p_a \left(\frac{\theta}{p_a}\right)^{k_2} \left(1 + \frac{\tau_{oct}}{p_a}\right)^{k_3}$$

b) Fit k_1 (modulus constant), k_2 (bulk stress sensitivity), and k_3 (shear stress sensitivity) using base modulus and computed stress states.

Step 5: Calculate Global Enhancement Ratios

a) Determine adjustment ratios for geogrid sections relative to the control:

$$\alpha = \frac{k_1^{GG}}{k_1^{Control}}$$

$$-\beta = \frac{k_2^{GG}}{k_2^{Control}}$$

$$-\gamma = \frac{k_3^{GG}}{k_3^{Control}}$$

Step 6: Assign Depth-Based Interaction Factors

a) Define MSL zone: typical ±4 in. from geogrid or 2 sublayers on either side of GG.
b) Assign interaction factors:

0.75 = full confinement (geogrid plane)

0.25 = partial confinement (adjacent sublayers)

0.0 = no confinement (no effect/others)

Step 7: Compute Sublayer-Specific Parameters

a) Modify base layer parameters using:

$$\boldsymbol{k_n} = (\mathbf{1} + [\boldsymbol{\delta} \times \boldsymbol{interaction}\mathbf{n}]) \times \boldsymbol{k_n^{control}}, \boldsymbol{where\ \delta} \in \{\boldsymbol{\alpha}, -\boldsymbol{\beta}, -\boldsymbol{\gamma}\}$$

b) Apply to k_1, k_2, and k_3 for all six sublayers.

Step 8: Calculate Composite Modulus for Validation

a) Use harmonic mean to compute effective layer modulus:

$$M_{R,eff} = \left(\sum_{i=1}^{n} \frac{h_i}{E_i}\right)^{-1}$$

b) Compare with APLT-measured modulus at each load stage.

Step 9: Simulate Pavement Response in Pavement ME/C-FLEX

a) Assign average modulus (Pavement ME) or calibrated sublayer resilient modulus model parameters (C-FLEX).

   I. For C-FLEX, Simulate typical stress conditions (e.g., 15 psi contact stress, 18 in. plate).
   II. For C-FLEX, Analyze stress distribution, deflection, and strain profiles.

(Optional) Step 10: Validate with Field Sensor Data

a) Compare:

Modeled deflections vs. repeated loading test results

Local stiffness vs. BE sensor vs. trends (if available)

Subgrade stress vs. earth pressure cell data (if available)

(Optional) Step 11: Finalize Design-Ready Inputs

b) Document calibrated parameters and sublayer distributions.
c) Generate adjustment tables for use in Pavement ME or future INDOT designs.
d) Recommend implementation of depth-varying modulus profiles in ME design of stabilized bases.

About the Joint Transportation Research Program (JTRP)

On March 11, 1937, the Indiana Legislature passed an act which authorized the Indiana State Highway Commission to cooperate with and assist Purdue University in developing the best methods of improving and maintaining the highways of the state and the respective counties thereof. That collaborative effort was called the Joint Highway Research Project (JHRP). In 1997 the collaborative venture was renamed as the Joint Transportation Research Program (JTRP) to reflect the state and national efforts to integrate the management and operation of various transportation modes.

The first studies of JHRP were concerned with Test Road No. 1—evaluation of the weathering characteristics of stabilized materials. After World War II, the JHRP program grew substantially and was regularly producing technical reports. Over 1,600 technical reports are now available, published as part of the JHRP and subsequently JTRP collaborative venture between Purdue University and what is now the Indiana Department of Transportation.

Free online access to all reports is provided through a unique collaboration between JTRP and Purdue Libraries. These are available at docs.lib.purdue.edu/jtrp/.

Further information about JTRP and its current research program is available at engineering.purdue.edu/JTRP.

About This Report

An open access version of this publication is available online. See the URL in the citation below.

Husain, S. F., Qamhia, I. I. A., Tutumluer, E., & Becker, P. J. (2025). *Resilient modulus improvements to bases and subgrades from geosynthetic reinforcement* (Joint Transportation Research Program Publication No. FHWA/IN/JTRP-2025/37). West Lafayette, IN: Purdue University. https://doi.org/10.5703/1288284318600